Aalto University
School of Engineering

European Mining Course

Harm Oosterbaan

Numerical thermal back-calculation of the Kerava Solar Village underground thermal energy storage

Master's Thesis
Espoo 26.08.2016
Supervisor: Prof. Mikael Rinne
Instructor: MSc Mateusz Janiszewski

Author Harm Oosterbaan

Title of thesis Numerical thermal back-calculation of the Kerava Solar Village underground thermal energy storage

Degree program European Mining, Minerals and Environmental Program (EMMEP)

Major/minor European Mining Course   **Code** R3008

Thesis supervisor Prof. Mikael Rinne

Thesis advisor(s) MSc Mateusz Janiszewski

Date 26.08.2016   **Number of pages** 72+5   **Language** English

Abstract

With increasing pressure to reduce the fraction of energy coming from fossil fuels, there is an increased need for research into feasible, and sustainable energy sources, such as solar energy. The problem with solar energy is the mismatch between supply and demand, and so the energy needs to be stored. This thesis is a part of the project titled "Tackling the Challenges of a Solar-Community Concept in High Latitudes", and aims in helping to design a thermal energy storage system for southern Finland that is economically feasible and has a high performance. For this purpose, a back-calculation of the underground thermal energy storage (UTES) of the Kerava Solar Village was performed. The main objective was to calibrate the numerical models to be used in an optimization by quantifying the thermal properties of the surrounding granite and soil.

The UTES of the Kerava Solar Village consisted of a rock pit filled with water and two surrounding rings of boreholes. From the 1st of June until the 31st of August 1984, the rock pit was continuously charged, and the energy flows from the boreholes were negligible. COMSOL Multiphysics 5.2® was used to create a model in which the temperature of the rock pit was used as the heat source and the heat propagation through the surrounding rock as the output to which the historical data was compared.

The best replication of the historical temperature inside the rock near the surface was achieved with a conductivity of 2.8 and 1.0 W/(m·K) for granite and soil respectively. When looking at the deeper sections, the best fit was obtained for a conductivity of 5.5 and 1.0 W/(m·K) for granite and soil respectively. These results are conflicting, and the realistic range of the conductivity for granite is 3-4 W/(m·K), and so the thermal conductivity could not be estimated with confidence.

The main problem throughout the back-calculation was the lack of data. To perform a successful back-calculation, all the parameters of the system need to be known, such as the geology, hydrology, and detailed technical drawings, but also the temperature distribution inside the heat source, and heat storage medium.

Keywords Back-calculation, Kerava Solar Village, Underground Thermal Energy Storage

Foreword

Table of contents

List of figures

List of tables

Nomenclature

a_m	Fraction melted	
a_r	Fraction reacted	
α_p	Coefficient of thermal expansion	1/K
Δh_m	Enthalpy of fusion	KJ/kg
Δh_r	Endothermic heat of reaction	KJ/kg
m	Mass	kg
ρ	Density	kg/m^3
T_i	Initial temperature	K
T_m	Melting temperature	K
T_f	Final temperature	K
T_{ext}	External air temperature	K
C_p	Specific heat with constant pressure	J/(kg·K)
C_{lp}	Average specific heat between T_f and T_m	
Q	Energy amount	J
q	Heat flux	W
h	Heat transfer coefficient	W/(m^2·K)
L	Characteristic length of area/perimeter	M
Ra_L	Rayleigh number	
g	Gravitational constant	m/s^2
μ	Dynamic viscosity	Pa·s
k	Thermal conductivity	W/(m·K)

1 Introduction

1.1 *Background*

With increasing pressure to reduce the fraction of energy coming from fossil fuels, there is an increased need for research into feasible and sustainable energy sources. One of those sources is solar energy. The problem with solar energy is that the supply and demand are negatively correlated. In the summer period there is an abundant supply of solar radiation but a low heat demand and in the winter months, this is reversed. A solution to this mismatch would be to store the energy into a system that gives the user the ability to take energy from the system when needed. This thesis is a part of the project titled "Tackling the Challenges of a Solar-Community Concept in High Latitudes".

1.2 *Objectives*

There are many different methods of storing thermal energy. The decision to build an energy storage system is based on the economic feasibility and the performance of the system. The purpose of this thesis is to aid in the design of a thermal energy storage system for southern Finland that is economically feasible and has a high performance.

To evaluate and optimize the performance of any system a simulation can provide great insight into the system. However to be able to trust the results of the simulation a back-calculation can be of great help. In this thesis, the Kerava Solar Village project will be back-calculated to calibrate the model. Measured data will be used as input, and the simulation output will be compared to measured data. When the output correlates to the measurements the confidence level of the simulated results will increase. The software that will be used is COMSOL Multiphysics 5.2®. The research questions related to this objective are:

- What data is available and useful for the back calculation?
- What data will be used as input data and to what will the results be compared?
- What time window will be used for each operational mode in the back calculations?
- How should the models be constructed?
- What are the resulting thermal parameters quantitatively?

1.3 *Scope*

The Kerava solar village project consisted of 44 terraced houses and a total of 1100 m^2 single-glazed flat plate collectors, capturing the solar energy. This energy was then stored in the underground rock pit and borehole storage. The system of interest in this thesis and the one that will be back-calculated is the underground thermal energy storage during a charging cycle.

1.4 *Structure*

Chapter 2 gives some general background information on the Kerava Solar Village and how the system was modeled in 1983. A short review of simulating thermal energy storages using COMSOL Multiphysics 5.2® is given before starting the main body of the thesis. The back-calculation begins in chapter 3 by cataloging the available data on the Kerava project. A time period is chosen for which there is enough data to use in the simulations. With chapter 3.3 the modeling begins by creating a simple 2D-model. This model is improved along the way, and a 3D-model is set up to implement the characteristics of the terrain, such as geology and topography. The results are presented and discussed after each separate model, and a recap of all discussions is given in chapter 4. The final conclusions are given in Chapter 5 and the recommendations in Chapter 6.

2 Thermal energy storage

2.1 *Thermal energy storage technologies*

Thermal energy storage systems are classified into three groups, representing different methods. These methods are sensible heat storage (SHS), latent heat storage (LHS) and thermochemical heat storage (THS). The energy in SHS is stored by raising the temperature of a solid or liquid. The amount of stored heat (Q) depends on the mediums specific heat capacity (C_p), the temperature difference (initial T_i, and final T_f) and the amount of storage material (m), and is described by the following relation (Sharma and Sagara, 2005):

$$Q = \int_{T_i}^{T_f} mC_p dT = mC_p(T_f - T_i).$$ (1)

Upon cooling this energy is released. No phase change takes place. In LHS the phase change is essential as the energy is absorbed or released when the medium, a phase change material (PCM) undergoes a phase change. The storage capacity of LHS system with a PCM medium is given by (Sharma and Sagara, 2005):

$$Q = ma_m \Delta h_m + \int_i^m mC_p dT + \int_m^f mC_p dT$$ (2)

$$= m \left[a_m \Delta h_m + C_{sp}(T_m - T_i) + C_{lp}(T_f - T_m) \right]$$

in which a_m is the fraction melted, Δh_m the enthalpy of fusion, T_m the melting temperature, and the C_{sp} and C_{lp} the average specific heat between T_i and T_m, and T_m and T_f respectively. Thermochemical heat is stored inside the medium as a chemical bond. There is a reversible chemical reaction that is either endo- or exothermic and the amount of stored heat is determined by the fraction that reacted (a_r), the endothermic heat of reaction (Δh_r) and the amount of storage material (Sharma and Sagara, 2005).

$$Q = a_r m \Delta h_r$$ (3)

The required amount of stored energy is significant, and thus the volume to contain this energy is large and according to Nordell and Hellstrom (2000) the most cost-effective method to obtain this volume is by using soil or bedrock as a sensible storage media. For solar thermal energy, the solar radiation is transformed into heat by the solar collectors. This heat is transported to the storage system and absorbed by the material as sensible heat. The amount of energy that can be absorbed by the system is dependent on the heat capacity, the volume, the density and the temperature difference between the initial and the final state, of the storage material.

There are multiple ways of constructing such a sensible storage system. Water is also a cost effective media as it is cheap and has a high thermal capacity. Systems using natural underground sites for storing energy are called Underground Thermal Energy Storage (UTES) systems. Among these UTES systems developed since 1970 are (Novo et al., 2010) (Figure 1):

- Aquifer thermal energy storage (ATES)
- Borehole thermal energy storage (BTES)
- Cavern thermal energy storage (CTES)
- Pit thermal energy storage (PTES)
- Water Tank (TTES)
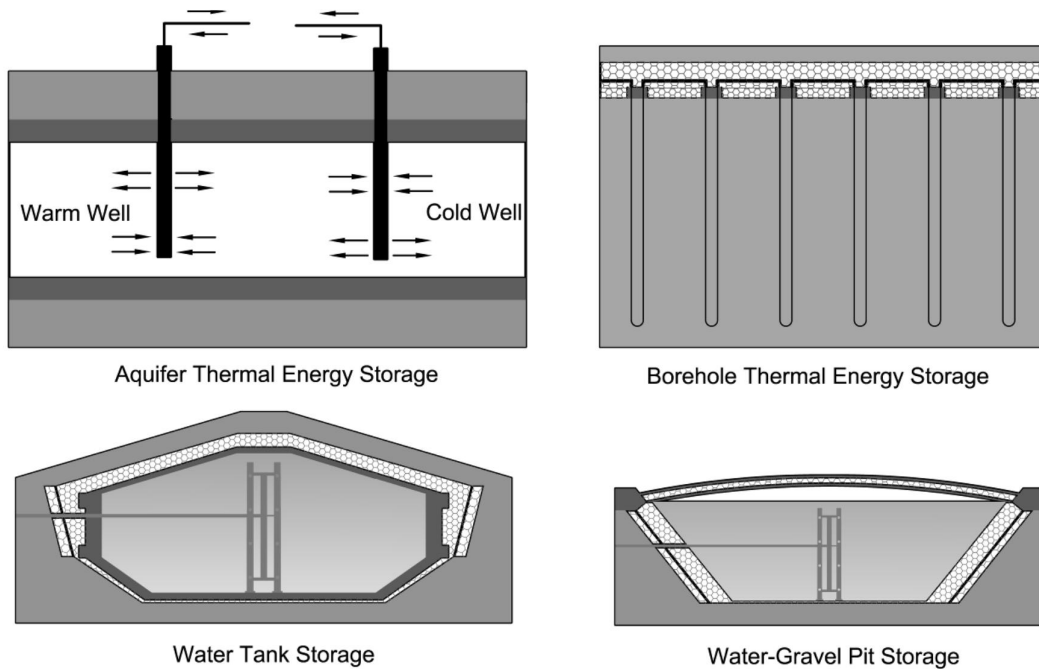
Figure 1. Underground thermal energy storage concepts (Pavlov and Olesen, 2011)

All except for BTES use water as the main storage media. BTES uses the ground as storage media. Heat is transferred to and from the rock through the use of heat exchangers inside the ground. The ATES uses a natural aquifer to store the energy. Two wells are connected to the aquifer and heat is injected in one and cold water is extracted from the other. During discharge, this cycle is reversed. The CTES uses large underground water reservoirs to store the heat. The pit and water tank storage are artificial structures built below or close to the surface, and they need insulation on the top and the sides. A detailed description of all storage systems and their advantages and disadvantages are given in a Master thesis written by Honkonen (2016).

The need for this insulation is what makes the pit and tank storages expensive, but the high heat capacity and excellent heat transfer properties are a significant advantage. A borehole heat storage has low costs but also relatively low heat capacity and heat transfer properties. A combination of the two promises operational advantages while reducing the

economic disadvantages. The combination can be less expensive because the pit does not need insulation on the sides as the heat loss from the pit is charging the borehole storage. The low heat transfer properties of the borehole storage will be compensated by the rock pit storage which will serve as a rapid response diurnal storage, and the borehole storage will serve as seasonal storage.
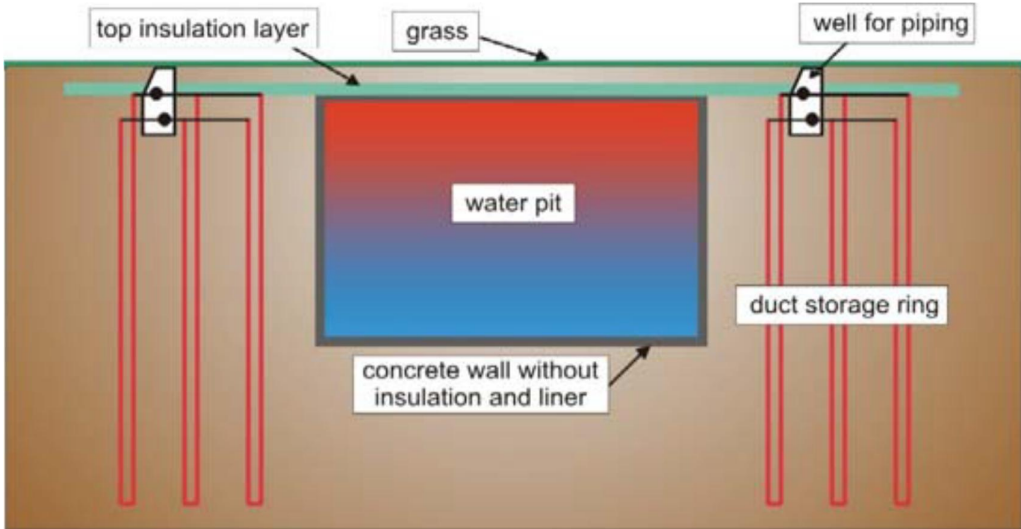
Figure 2. Combined water pit and borehole storage (Reuss et al., 2006)

In Attenkirchen, Germany, such a combination system has been realized and is in operation since 2002. It consists of a 500 m^3 water store with 90 borehole heat exchangers of 30m depth surrounding it, giving a rock volume of 10,500 m^3, which corresponds to 6,800 m^3 water equivalent (Figure 2). The water store was made of pre-stressed concrete, and the surrounding geology consists of a sequence of clay and silt layers with low permeability (Reuss, 2015). A solar fraction, i.e. amount of energy provided by the solar technology divided by the total energy required, of 74% has been reached even though there were significant operational problems related to the control program which caused certain features and operation modes unavailable for testing. Despite these problems, the system showed to be technically and economically feasible (Reuss et al., 2006). The Kerava Solar Village in Kerava, Finland, is another example of a combination storage and will be discussed further in the next chapter.

2.2 *Kerava Solar Village*

The Kerava solar project is the first Finnish solar district heating system using seasonal heat storage. The undertaking was started in 1979 when SITRA (The Finish National Fund for Research and Development) financed the preliminary study. The actual project was financed by SITRA, the Ministry of Trade and Industry, the National Housing Board, the Ministry of the Interior, various banks and the Imatra Power Company but owned privately. It is located in the town Kerava, about 35km North of Helsinki (60°N).

Figure 3. Map of Finland showing the location of the Kerava Solar Village (Google, 2016)

The solar village as described by (Lund et al., 1983; Mäkinen and Lund, 1983; Lund et al., 1984; Fryer, 1985; Lund, 1986; Peltola, 1986; Lund, 1987; Peippo and Peltola, 1988) consists of a solar-assisted heat pump and a rock pit heat store. The rock pit water store has a volume of 1500 m^3. Borehole heat exchangers are drilled around the water store to recover the heat loss partially. The boreholes are drilled in two circles around the water store. The inner circle consists of 18 boreholes to a depth of 22m and at an angle of 12°. The outer circle has 36 boreholes to a depth of 24m at an angle of 24°. A graphical representation is presented in Figure 4. The heat loss was recovered by circulating cold water coming from the heat pump evaporator through the holes before returning the water to the bottom of the water store (Fryer, 1985).

22
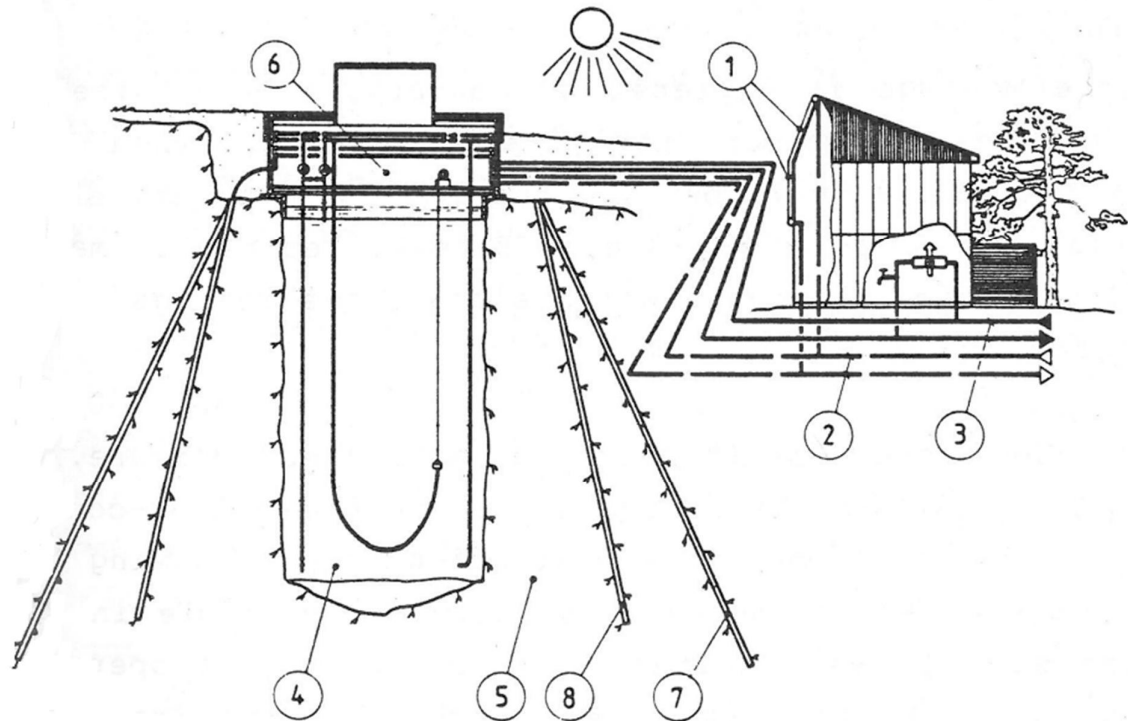
Figure 4. Heat storage and piping network. 1) Solar Collectors. 2) Fluid distribution network. 3) Heat distribution network. 4) Hot water storage. 5) Rock storage. 6) Heating plant. 7) Outer circle of boreholes. 8) Inner circle of boreholes (Fryer, 1985)

The water inside the tank was stratified with hot water at the top and cold water at the bottom. Water returning to the tank is injected into the corresponding temperature layer through the use of an automated winch. Cold water from the bottom is circulated to the collector's loop. With the heat pump running, this water is cooled even more by the evaporator increasing the collector's efficiency. An electric boiler is used whenever the temperature at the top of the tank falls below 65 °C at night and 50 °C during the day. The same goes for the heat pump, which transports energy from the bottom to the top of the tank. However, they are never run in conjunction to reduce the peak electricity load. The rock store is charged whenever the water store has reached an average temperature of over 50 °C. This however never happened as the maximum average temperature in 1984 was 49.5 °C. The storage capacity of the 1500 m^3 water tank was 100 MWh. The 11.000 m^3 rock store only has the same effective storage capacity of 300 m^3 of water (Fryer, 1985). This figure might be so small because the rock was not actively charged but only used passively to recover the heat loss during operation.

The system was monitored during its operation from 1983 till 1986 and the main findings are shown in Table 1. Because of operational difficulties the boreholes were only used passively and in 1984 they connected the two borehole circles in series to improve the heat recovery during discharging. The pipes recovered about 25% of the heat loss from the water store, which could have been higher if not for the malfunctions in the heat pump's operation. The pipes had an output of on average about 20 W/m or 4-5 W/(K·m). As the borehole storage was not actively charged the water store became the main storage. Due

to its limited capacity, it became fully charged by the end of May and thus the rest of the summer solar energy was dissipated. This dissipated energy was estimated to amount to 90 MWh, which was 30-35% of all collected solar energy. When this energy could have been charged into the borehole storage, the solar fraction of the system could have been 27-31% instead of the achieved 21% (Lund, 1988).

Table 1. Measured storage performance in Kerava Solar Village (Lund, 1987)

Year	Water storage losses (MWh)	Water storage efficiency without pipes (%)	Recovered by pipes (MWh)
1983	140	63	3
1984	134	80	51
1985	179	76	60

As mentioned before, the rock storage would only be charged when the average temperature of the water store would reach 50 °C. The maximum average temperature of the water store reached 49.5 °C during the summer of 1984 (Fryer, 1985). Lund (1988), wrote that the water store was completely charged by the end of May and that the remaining solar energy was dissipated as such. This sounds contradictory, but P. Lund gave an explanation (personal communication, 1st June 2016) as the system was designed for a high-temperature solar collector field but because of delivery problems medium temperature solar collectors were installed. This meant that the water store temperature could never reach its intended level and thus was fully charged too early. The purpose of the project was research. It was a test case for the innovative combination of boreholes and rock pit storage. It was however not a true combination of the two different thermal energy storage systems. The boreholes were merely used for extracting the heat loss, from the rock pit thermal energy storage system, and not for actively charging of the rock mass.

2.3 *Numerical modeling in 1983*

Before the Kerava Solar Village was taken into operation, simulations were run to determine the system performance under different weather conditions over a period of several years. The effect of various degradation mechanisms on the system was also considered. The degradation mechanisms considered were failing of heat pump and decreasing effective solar collector surface. For the different weather conditions, the average ($\overline{K}$), minimum (K_{min}), and maximum (K_{max}) monthly solar radiation availability were considered. The values were determined using data over the previous 10 years (Lund et al., 1983).

They assumed a hot water demand of 180 MWh per year and an annual heating requirement of 294 MWh with average solar radiation. The condenser of the heat pump would put out just over 60 % of the annual heat energy demand. For the different solar

radiation availabilities, the energy received on the collector surfaces per year was for $\overline{K}$, K_{min}, and K_{max}: 670, 933 and 1162 kWh/m^2. The heat self-sufficiency would be 45.8, 61.6, and 72.9 % respectively (Lund et al., 1983).

The first deterioration mechanism that was considered was the shut-down of the heat pump. The need for direct auxiliary energy increases significantly and the solar collector yield was reduced. The solar fraction without the heat pump would be only 30 %. The second deterioration mechanism was the reduction of effective solar collector surface. The effect was smaller than the shut-down of the heat pump, because when the surface area reduces the remaining surface will have a higher efficiency due to a larger ratio of store size to surface area. With a 50 % surface reduction, the solar fraction would go down to 50 % from 61.6 % (Lund et al., 1983).

The heat loss from the water store into the rock would be 88.4 MWh annually under normal conditions. The boreholes in the outer circle should be recovering 42 % of this energy. Without the heat pump, the heat loss would be 109 MWh (Lund et al., 1983).

According to the simulations of Lund *et al*. (1983), the thermal capacity of the water store should reach its maximum in late July. In the middle of December, the water store would be almost completely discharged, and auxiliary energy is increased. The electric boiler would be needed from December to late February. They concluded that to reduce the use of the electric boiler the amount of stored heat should be increased by increasing the solar collector area or by using the boiler in late autumn to charge the water store. In the present configuration, there would not be enough heat to charge the rock store during the charging period.

2.4 *Finite Element Method and COMSOL*

COMSOL Multiphysics 5.2® software package uses a Finite Element Method (FEM) to evaluate models. It provides the user with a powerful tool in design. The finite element method divides a domain into a specific number of elements making up the mesh, which is why it is called a finite method. Because the elements are not infinitely small, the solution can only be an approximation. Nonetheless, when the dimensions of the mesh are chosen carefully, the result is close to reality.

Rapports such as (Chiasson, 2010; Kim et al., 2010; Corradi et al., 2008; Schiavi, 2009; Johansson et al., 2012; Lanini et al., 2014), describe multiple applications of COMSOL in modeling thermal energy storage and make COMSOL one of the preferred commercial software packages used for this purpose.

The use of COMSOL Multiphysics has been validated in reports involving thermal storages. One such report made by Oberdorfer *et al.* (2013) describes the modeling of a double U-tube Borehole Heat Exchanger (BHE).
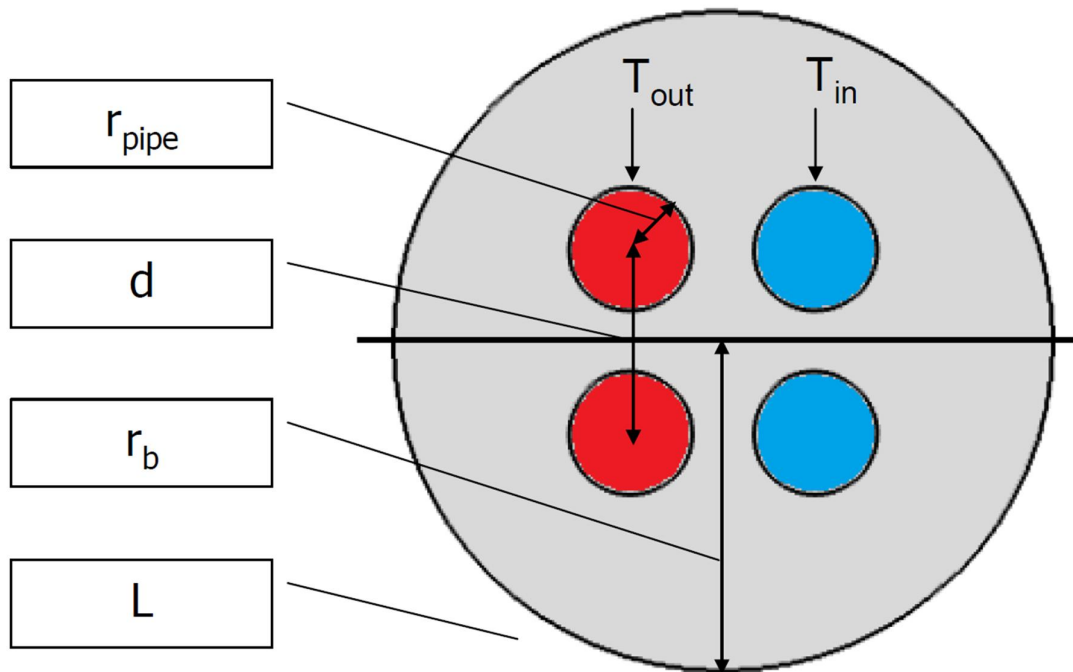
Figure 5. Top view on the Double U-tube BHE design (Oberdorfer et al., 2013)

The model was validated by comparing the results to an existing test site containing a BHE array. The main thermal property of interest was the thermal resistivity of the BHE and the modeled value returned 0.09 (m·K/W) where the experimental results from the test site yielded a range of 0.07-0.119 (m·K/W) and thus validated the model. They then continued to do parametric studies. The thermal conductivities (k) of the materials used in the BHE and the fluid itself, including its viscosity, were changed as well as the geometric properties to see their influence on the thermal resistivity.

3 Back calculation of Kerava Solar Village

3.1 *Available Data*

The Kerava Solar Village was monitored using 141 measuring points. They monitored temperatures in the piping system, the water store and inside the surrounding rock mass as well as energy flows. The heating plant contained 108 sensors, the homes and collector groups 30 and for the weather three sensors were employed.

Peippo and Peltola (1988) published the results for each year from 1983 until 1986. Because most of the temperature graphs are distributions and display frequency percentages instead of temperature against time, their usability is limited. For a back-calculation to be effective, the initial state needs to be known as well as the path taken to the final result. With graphs that are not time-based, this is impossible to assess accurately.
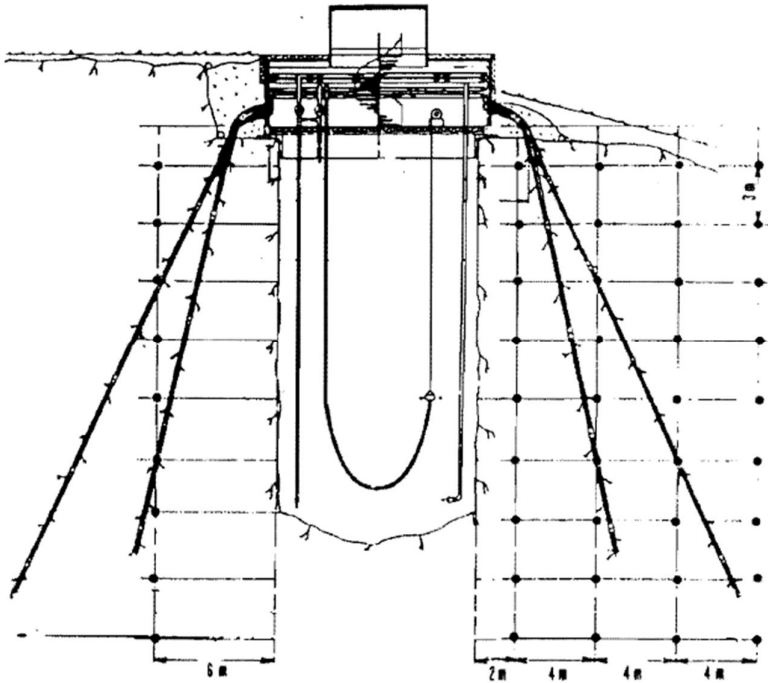
Figure 6. Sensor placement inside the rock. In the Northern direction at 2 m, 6 m, 10 m, and 14 m from the water store. In the East, South, and West direction only at 6 m from the water store. Placement up to 24 m in depth at an interval of 3 m

For this thesis, only the 18 sensors inside the water store and the 63 inside the rock are relevant (Figure 6). In a report published by Peltola (1986) a graph is displayed of the surrounding rock temperature in different directions and distances from the water store. Figure 7 is one of those graphs which shows the temperature in the rock at depth over time in the northern direction, 2 m away from the water store. The temperatures are displayed from the start of the operation in 1983 until the end of 1985. Among the data in Peippo (1988) is a graph which shows the isotherms inside the water tank (Figure 8) during 1984

27

and a graph displaying the outside temperature over 1984 (Figure 9). These graphs will be used for the first simulation of the Kerava Solar Village.

1st of June till 31st of August
1984
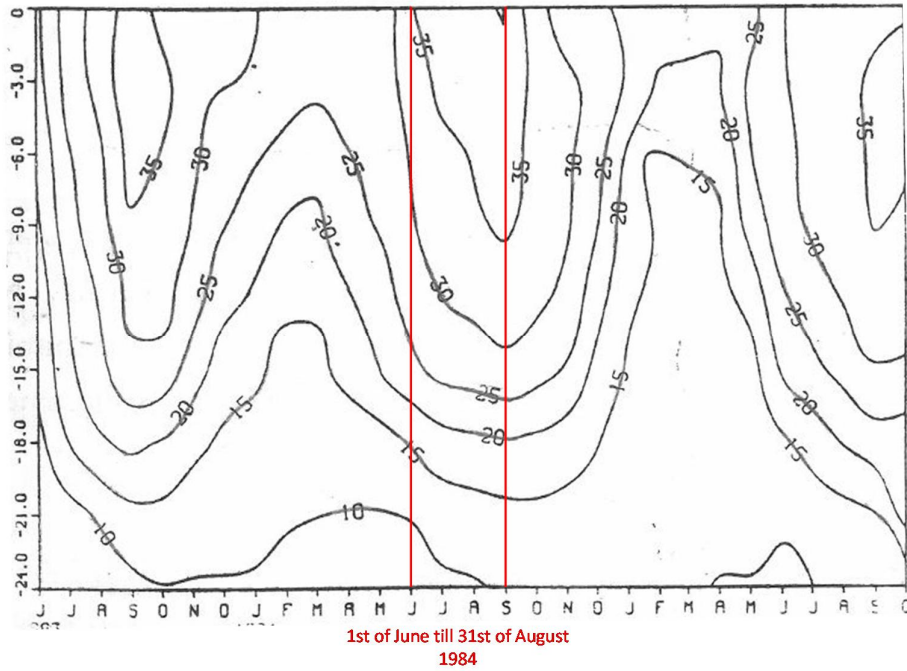
Figure 7. Isotherms of rock mass at 2m distance from water store in a Northern direction from 1983-85 (Peltola, 1986)

WATER STORAGE TEMPERATURES
1984

1st of June   31st of August

TEMPERATURES —— 10 —·— 20 —— 30 — — 40 —— 50 ······· 60 —— 70
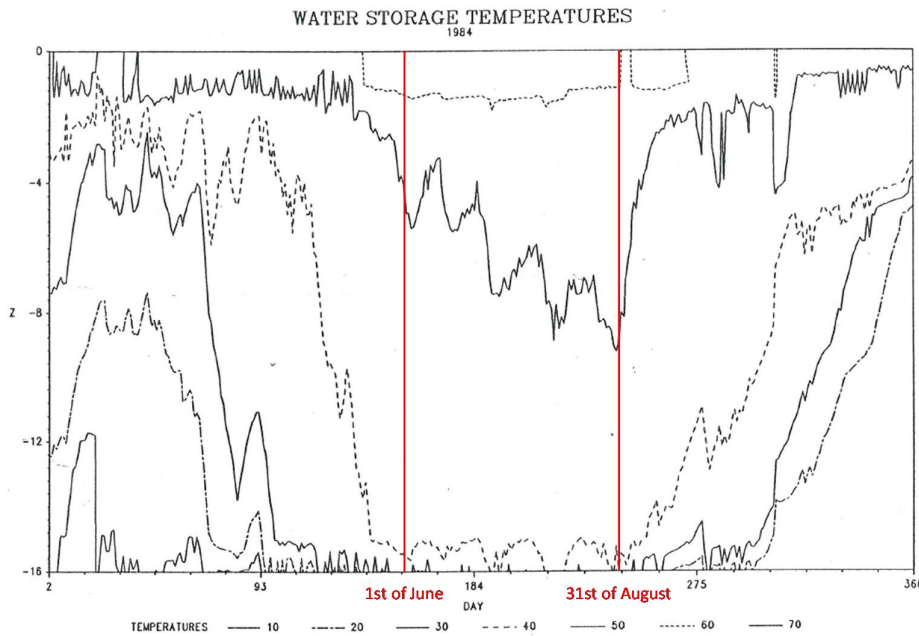
Figure 8. Isotherms inside water store 1984 (Peippo and Peltola, 1988)

28
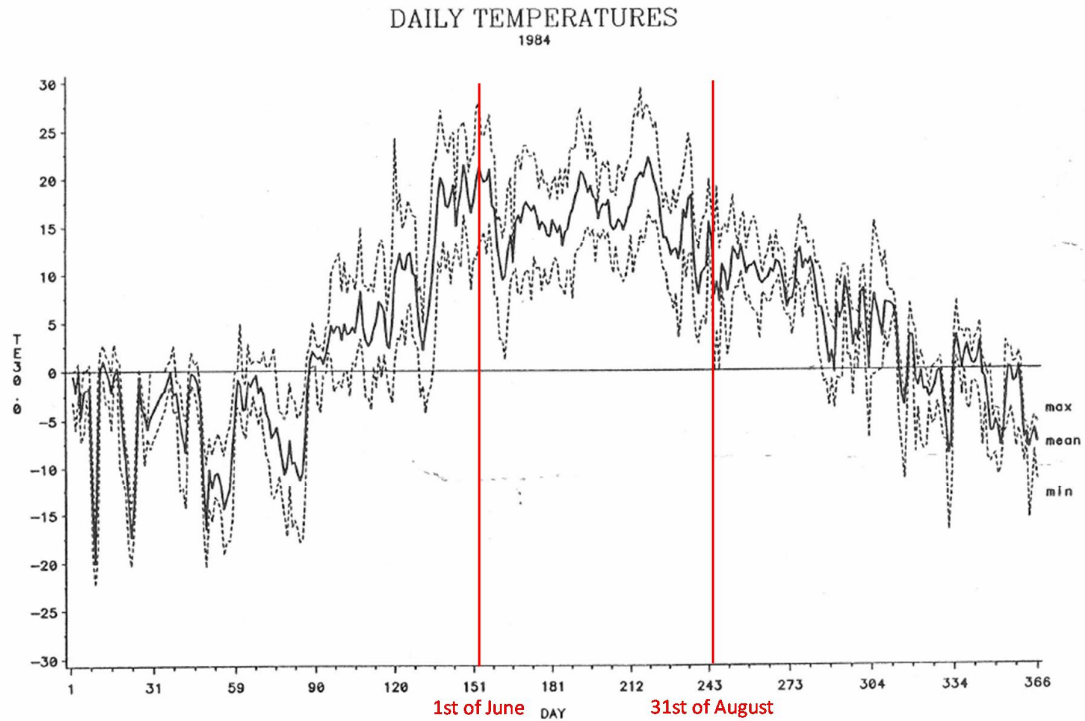
Figure 9. Outside daily temperatures in 1984 (Peippo and Peltola, 1988)

3.2 *Continuous charging of the water store*

The isotherms inside the water store are illustrated in Figure 8 for 1984, and Table 2 shows the energy flows in different sub-systems during 1984. For the first simulation, the temperature of the water store and the outside air temperature will be used as input and the heat propagation through the rock mass as output. To be able to compare the simulated results to the actual results, the operating conditions need to be set equal. During operation, the water coming from the evaporator is returned to the bottom of the water store, but sometimes it is fed through the outer bore holes to get heated before returning to the water store. This will take heat from the rock mass and thus needs to be taken into account. During June, July, and August of 1984 this amount of energy is very limited as seen in Table 2. Therefore, this period is chosen for the simulation, as the energy flow from the inner borehole circle is also zero.

Figure 7 shows the Isotherms of the rock mass at 2m distance from the water store in the Northern direction from 1983-85. This graph, as well as the other rock temperature graphs from Appendix 1, is used to set the initial temperature of the rock in the model and to compare the results of the final state.

Table 2. Energy flows for different sub-systems during 1984 with all numbers in kWh (Peltola, 1986)

Month	Total	Solar collector	Condenser	Evaporator	Compressor	Boiler	Outer bore holes	Inner bore holes
Jan	73600	400.00	103260	70500	36400	23110	2900	1.0
Feb	74100	12200	149221	98200	56690	11090	5100	0.0
Mar	70100	33100	127182	83100	48980	7730	6000	-8.1
Apr	44500	36700	81306	54000	30340	2740	3900	2.0
May	24200	38700	45634	31000	16260	2110	2900	1.0
June	17000	28300	38356	25900	0	0	500	0.0
July	3600	6700	8152	5200	0	0	100	1.0
Aug	17700	23000	31107	19200	13290	0	800	1.0
Sep	32100	6200	41734	24500	19150	0	3800	1.0
Oct	45800	10100	72955	44200	31950	80	7200	65.0
Nov	44700	600	60807	37200	26230	140	5000	15.3
Dec	73300	200	116335	72100	4096	450	9100	3.9

Figure 8 of the temperature inside the water store has been digitized using Plot Digitizer which creates points according to predefined axes and scales. The points of the relevant period, have been loaded in MATLAB, and a curve has been fit through them. Subsequently, for every day the depth of each isotherm is stored, and a linear curve is fitted through them describing the temperature at all depths for every day. Because the data only describes isotherms and only until a depth of 16 m some assumptions need to be made for the temperature at the top and the bottom of the water store. The temperature at the top is set to 65 °C because the boiler has a set point at that temperature (Fryer, 1985). The temperature at the bottom is set to 15 °C as it is the main charging period and according to Fryer (1985) that is the maximum temperature at the bottom. Now the temperature at different depths can be modeled over time, and the result is shown in Figure 10. MATLAB is then used to write an Excel file with three columns. The first will hold the day number, the second the depth and the third the temperature. This table can be imported into COMSOL and with the interpolation function, all intermediate values are interpolated linearly. The full table is given in Appendix 2.
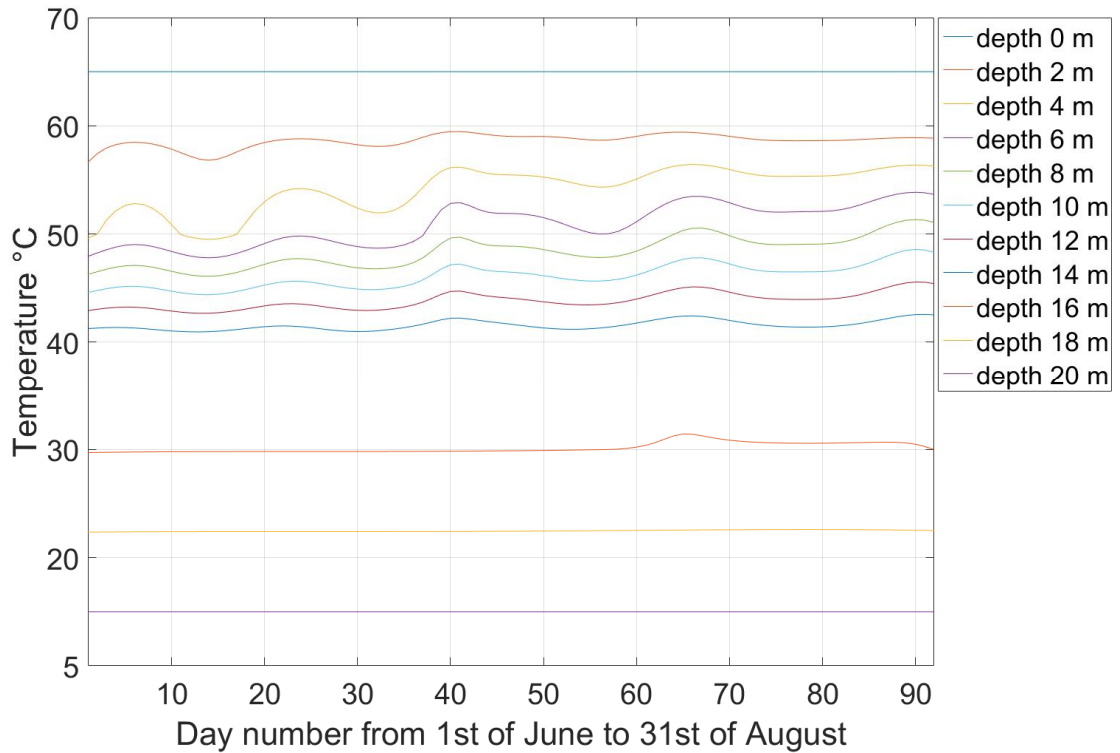
Figure 10. Temperature at different depths from the 1st of June till the 31st of August 1984

The outside temperature has been digitized the same way, and a curve is fitted through, describing the mean temperature. The result is given in Figure 11. Because there is much more variability in the real data than the best-fitted curve, the raw data is imported and interpolated linearly into COMSOL.
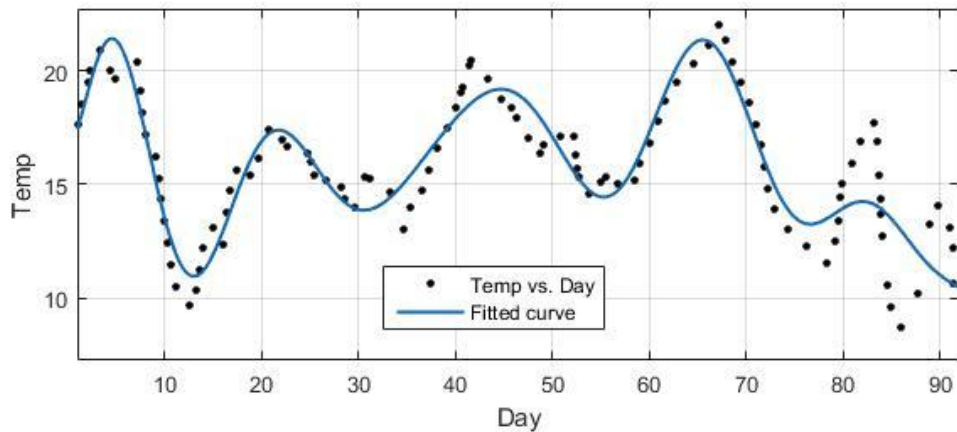
Figure 11. Fitted curve to describe the outside temperature from the 1st of June till the 31st of August 1984

For the initial rock temperatures, the depth of each isotherm is taken at all distances from the water store in the Northern direction and interpolated linearly in COMSOL. Only the Northern direction is imported into COMSOL because the model is 2D axisymmetric and

31

the amount of data is greatest in that direction, and the graphs do not differ much with regards to the other orientations.

3.3 *First 2D-axisymmetric model*

The heat transfer in solids physics module is chosen for the simulation. It requires three thermal properties assigned to all domains, i.e. the thermal conductivity (k), heat capacity (C_p) and density (ρ) to solve the heat equation:

$$\rho C_p \frac{\partial T}{\partial t} + \nabla * q = Q \qquad (4)$$

$$q = -k\nabla T \qquad (5)$$

Eppelbaum *et al*. (2014) give a worldly average conductivity for granite of 2.68 W/(m·K) over 383 samples and a heat capacity of 790 J/kg·K. Robertson (1988) shows a range of conductivities between 2 and 4 W/(m·K). Kukkonen and Peltoniemi (1998) did a study and found a range of thermal conductivities for Finish granite samples between 1.6 and 5 W/(m·K) where the mean was 3.5 W/(m·K) and the standard deviation 0.5 W/(m·K). A value for the heat capacity was not given in the rapport. A study done by Kukkonen (2015) shows an average thermal conductivity, heat capacity, and density of 3.0 W/(m·K), 714 J/kg·K and 2635 kg/m^3 respectively. This was an average of 10 pegmatitic granite samples taken from drill holes in Olkiluoto, Finland. As the Hukkonen (1998) report was on granite samples from all over Finland, this value of 3.5 W/(m·K) will be used, instead of the 3.0 W/(m·K) for a single location in Finland, in the simulation. For the heat capacity, a value of 714 J/kg·K will be used and a density of 2635 kg/m^3.
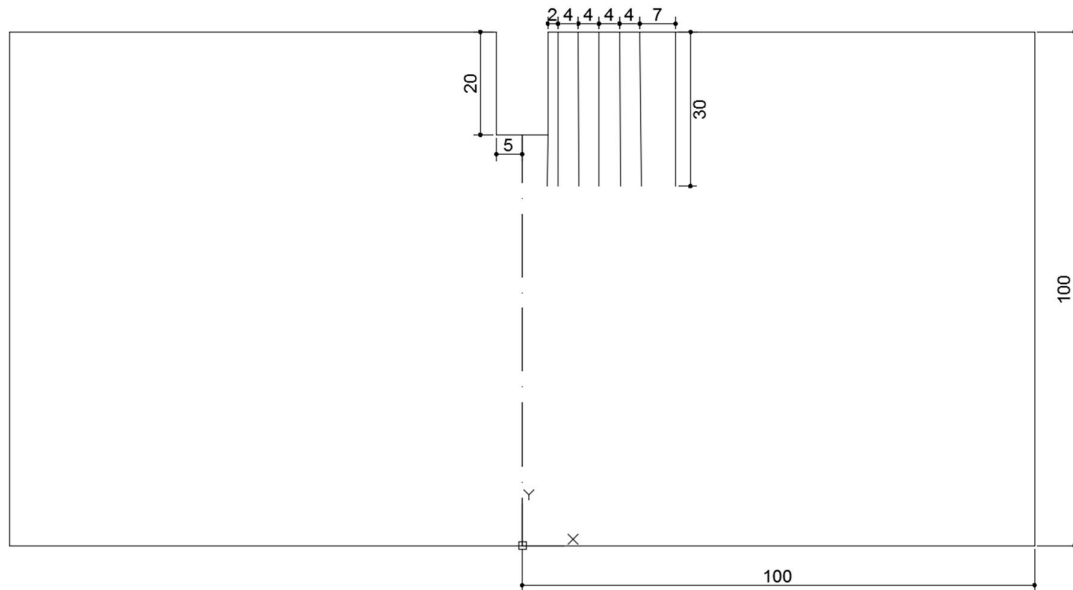
Figure 12. 2D-axisymmetric model layout with water store in the center and locations of initial rock temperatures at distances of 0, 2, 6, 10, 14, 18, and 25 m from water store. All values are in m

Because the first model is not very complex and the initial rock temperatures are equal in all directions, a 2D-axisymmetric model is made in COMSOL. Parameters are introduced that describe the dimensions of the system. Building the geometry using parameters, enables the user to alter them easily and investigate the changing results. The granite bedrock is modeled as a square with a height (z) of 100 m and a radius (r) of 100 m. With the water store having a height of 20 m and radius of 5 m, the size of the granite will ensure the boundary conditions will not affect the heat propagation. The initial temperature values for the granite domain are taken from the data presented by Peltola (1986).

Table 3. Initial rock temperatures used in COMSOL

Distance from water store													
0m		2m		6m		10m		14m		18m		25m	
Z (m)	T (°C)	Z (m)	T (°C)	Z (m)	T (°C)	Z (m)	T (°C)	Z (m)	T (°C)	Z (m)	T (°C)	Z (m)	T (°C)
0.0	65.0	0	31.2	0	14	0	9.5	0	8	0	8	0	8
-2.0	58.4	-3	31	-4	15	-4.5	10	-6	9	-12	8	-12	8
-4.0	52.6	-6.75	30	-8.5	16	-10	10.5	-24	6.5	-24	6	-24	6
-6.0	49.0	-10	28.5	-12.9	15	-15	10	-30	5.3	-30	5.3	-30	5.3
-8.0	47.1	-13.8	25	-20.3	10	-22.5	7						
-10.0	45.2	-16.4	20	-24	7.5	-30	5.3						
-12.0	43.3	-18.2	15	-30	5.3								
-14.0	41.4	-21.4	10										
-16.0	29.8	-24	7.5										
-18.0	22.4	-30	5.3										
-20.0	15.0												
-22.0	10.0												
-24.0	8.0												
-30.0	5.3												

The initial temperature at the boundary to the water store is set to be equal to the water store temperature. As the data only includes isotherms, some added values have been estimated, either interpolated or assumed to be going down to the stable rock temperature at depth. In Helsinki, Finland the average air temperature between 1974 and 1984 was 5.3 °C (Finnish Meteorological Institute, 2016) and so the rock temp at depth will resemble that number as Kerava is very close to Helsinki. The temperature gradient is not used for the undisturbed rock as it is the initial simulation. The full table that is used as input in COMSOL can be seen in Table 3. Inside the global definitions, an interpolation function is created that reads the data and interpolates linear and extrapolates constant. The result is shown in Figure 13.
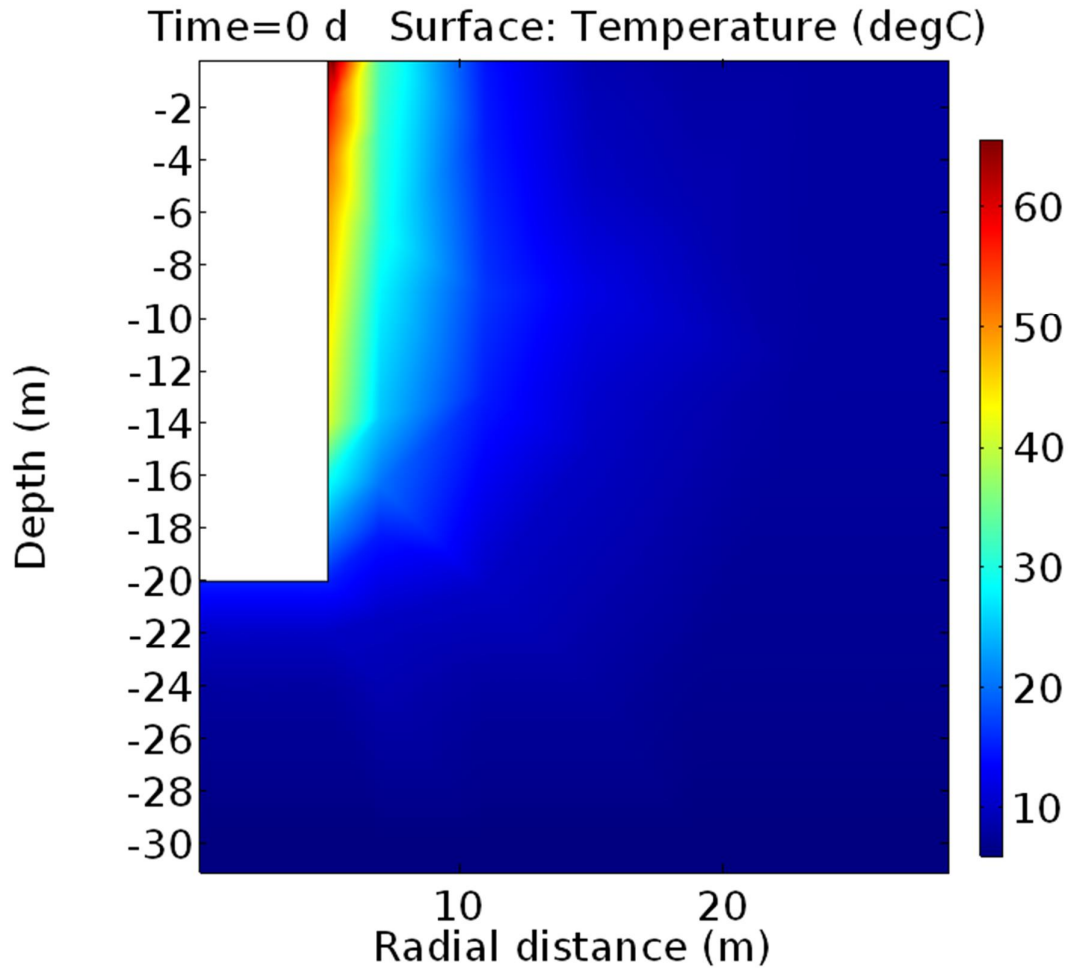
Figure 13. Initial temperature state of granite (°C)

For this first simulation, the water store temperature is used as a heat source and the heat propagation is the output that will be back-calculated. To model the water store, two temperature boundaries are incorporated - one for the side of the store and one for the bottom. The temperature on those boundaries is described by an interpolation function dependent on time and depth as shown in Figure 14. The data is taken as discussed from the isotherms in the northern direction.
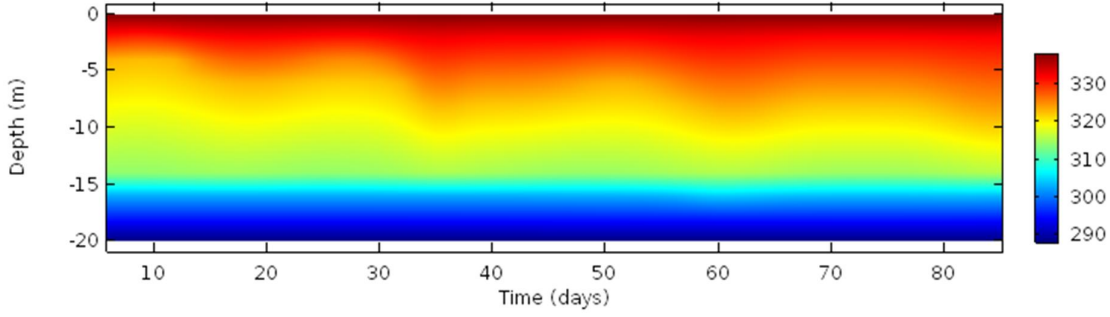
Figure 14. Temperature of the water store over time in (K)

The convective heat loss at the surface is set up as a heat flux boundary and is modeled as an external natural convection on the upside of a horizontal plate. The equation used is:

$$q = h(T_{ext} - T) \tag{6}$$

where if $T > T_{ext}$ then

$$h = \begin{cases} \dfrac{k}{L} 0.54 Ra_L^{1/4} \ if \ 10^4 \leq Ra_L \leq 10^7 \\ \dfrac{k}{L} 0.15 Ra_L^{1/3} \ if \ 10^7 \leq Ra_L \leq 10^{11} \end{cases} \tag{7}$$

if $T \leq T_{ext}$ then

$$h = \frac{k}{L} 0.27 Ra_L^{1/4} \ if \ 10^5 \leq Ra_L \leq 10^{10} \tag{8}$$

Where

$$Ra_L = \frac{g \alpha_p \rho^2 C_p |T - T_{ext}| L^3}{k\mu} \tag{9}$$

In which:
- T_{ext} is the temperature of the air
- h is the heat transfer coefficient (W/(m²·K))
- L is the characteristic length of area/perimeter (m)
- g is the acceleration of gravity (m/s²)
- k is the thermal conductivity of the fluid (W/(m·K))
- ρ is the air density depending on the absolute pressure (kg/m³)
- μ is the dynamic viscosity of air (Pa·s)
- C_p is the heat capacity at constant pressure of the fluid (J/(kg·K))
- α_p is the coefficient of thermal expansion as $1/T$ (1/K)
-

The characteristic length $L = \frac{\pi 100^2 - \pi 5^2}{2\pi 100 + 2\pi 5} = 47.5$, the absolute pressure is taken to be one atmosphere and the external temperature is taken from Figure 11. The remaining boundaries (side and bottom) are set to adiabatic insulated boundaries.

The free triangular mesh with normal mesh size is chosen with a minimum element size of 0.03 m, a maximum of 6.7 m and an element growth rate of 1.3. For post-processing purposes, three vertical lines are created at 2, 6, and 10 m from the water store. The

distance of these lines is chosen to match the distances of the temperature sensors in the Kerava case. A mesh distribution of 299 elements (300 nodes) is created along those lines to increase the plot precision. The introduction of these distributions of elements governs the mesh inside the region of interest, close to the water store, and thus a finer mesh size will not make a difference to the results, and a coarser mesh is not needed because the simulation runs in seconds. The mesh contains 22 954 elements with an average element quality (quantifies the regularity of the shapes of the mesh elements from 0 to 1, with 1 being the highest) of 0.9487. The used mesh is shown in Figure 15.
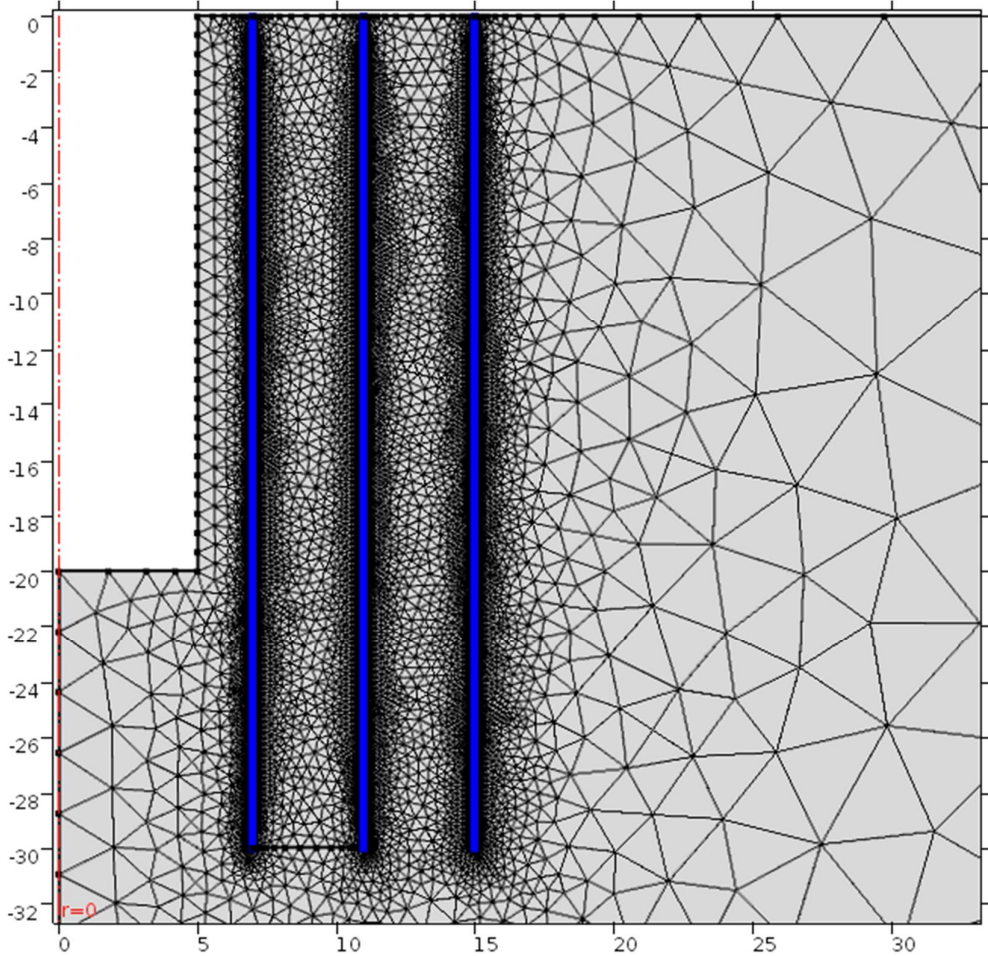
Figure 15. Mesh with indicated (blue) cut lines at distance 2, 6 and 10m from water store

The study is time dependent starting from 0 and going until 92 days with a time step of one day, representing the period in 1984 from the 1st of June until the 31st of August. The time steps taken by the solver are set free but only the specified time steps are stored for post-processing.

3.3.1 Results of the first simulation

To compare the results of the simulation to the historical data a plot needs to be created that displays the isotherms and their change in depth over time. The historical data has been digitized earlier according to Peltola (1986) and for the first comparison, the graph depicting the isotherms at a distance of 2m from the water store in the Northern direction is used. To create a similar plot out of COMSOL, a few tricks need to be employed. First, a new data set needs to be created which contains the data at 2m distance from the water store. For this, a cut line is created as shown in Figure 16.
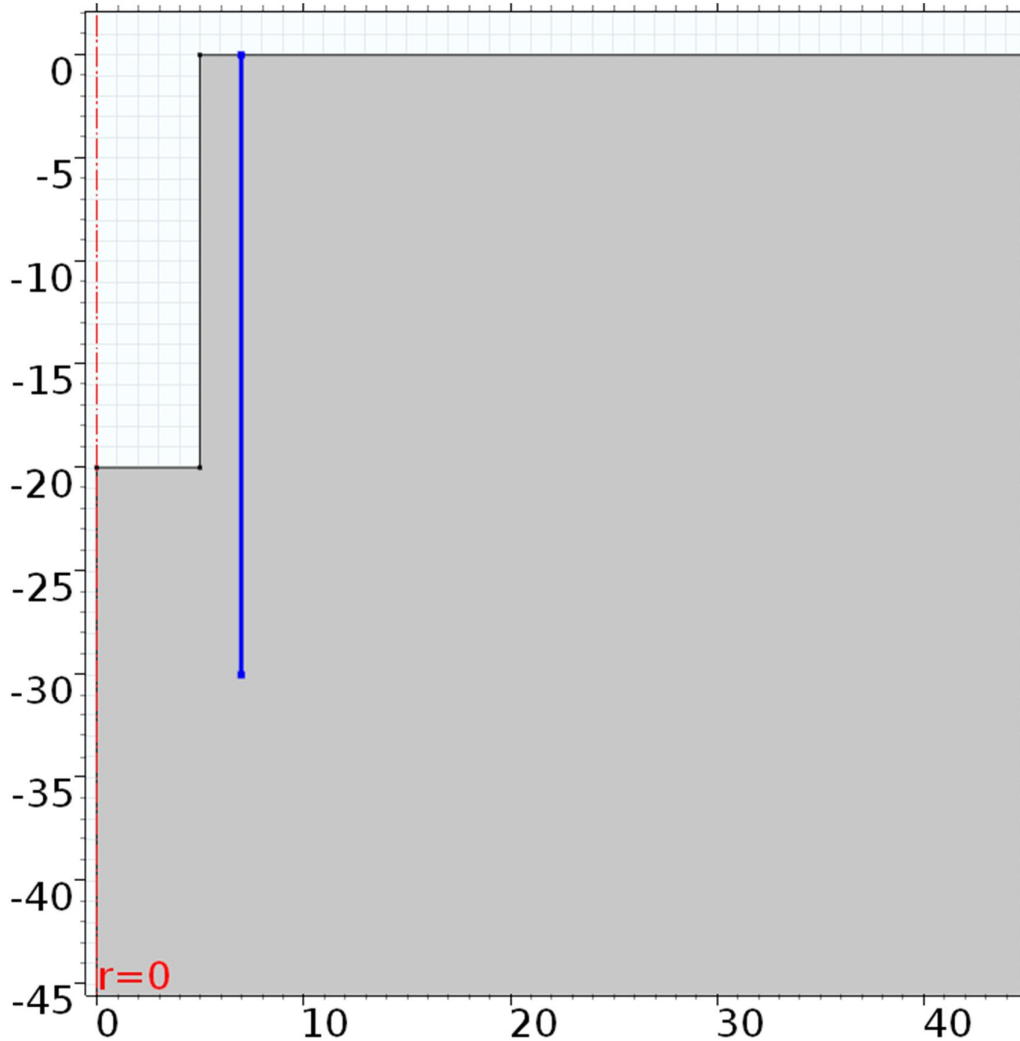
Figure 16. Cut Line 2D (blue) dataset creation at 2 m distance from water store and ranging in depth from 0 to 30 m

The data set now contains for each node on this cut line its temperature for all 92 days. A line integration could now be used to find the depth of each isotherm by setting the expression to temperature > isotherm (T_{iso}). This will return the length of the cut line for which the temperature is larger than the set T_{iso}. This, however, does not work here

because the isotherm folds back on itself. The temperature increases with depth at first but then decreases until it reaches the bottom, so the result of the line integration will have nothing to do with the actual depth. COMSOL does not seem to have a plot function that gives the desired result. To solve this, the cut line dataset is exported as a .txt file and imported into MATLAB by using the COMSOL Livelink with MATLAB. The .txt file contains the radial distance and depth of each node and the corresponding temperatures for each day. An algorithm is created that locates the depth, starting from the top, at which a certain isotherm is surpassed and interpolates between that depth and the one before to get the actual depth of the isotherm. This procedure is repeated starting from the bottom to get both depths. The result is shown in Figure 17.
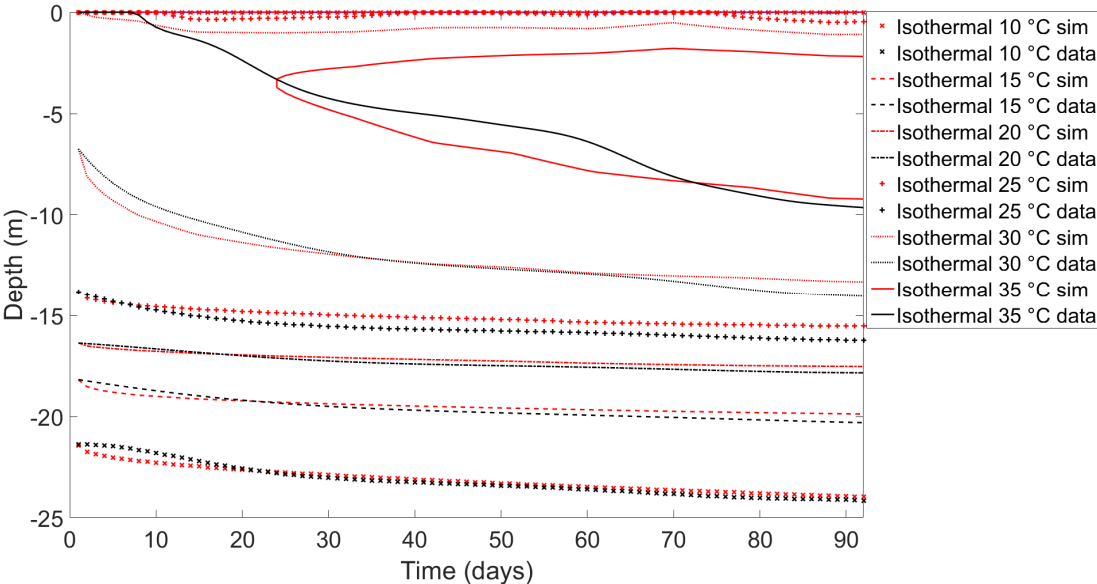
Figure 17. Comparison of the simulated isotherms depths against historical data in °C

3.3.2 Discussion of the first simulation

As seen in Figure 17, there is a difference between the simulated results and the historical data. The main difference is the folding back of the isotherms 35, 30 and 25 °C. This means that the top of the rock storage is cooling down too much, which could be caused by the absence of an insulating layer such as soil. Another difference is that the simulated isotherms do not get down to the same depth as the historical ones. This could be due to a lower than actual thermal diffusivity or an existing heat transportation process that has not been modeled. An example of which could be a fault where percolating meteoric waters distribute the heat downwards. When looking at the 35 °C historical isotherm at around 60 days, there appears a sudden increase in depth. This can only be explained by an increase in temperature differential. When looking at the water store temperature, the heat source, there is an increase in temperature that starts just before the rock temperature increase. However, this does not translate to an increase in the simulated temperature as it does for the historical data. This could indicate the presence of a different, unknown heat source or a leakage of hot water from the water store into the surrounding rock through faults, which opened up because of thermal expansion.

3.4 *Second model including soil*

As discussed before, a possible explanation for the folding back of the isotherms could be the absence of a soil layer. In this chapter, the thickness of such a soil layer will be explored as there was no historical data on the matter at this stage. A soil layer is added, and the thickness is varied during a parameter sweep. A material is assigned to the newly made domain with a density of 1700 kg/m^3 for average Finish soil, and with a water content of around 15%, the heat capacity at constant pressure can be calculated using:

$$C_{vs} = \frac{\rho_s}{\rho_w}\left(0.18 + 1.0\frac{w}{100}\right) * C_{vw} = 2412.3 \; KJ/m^3K \tag{10}$$

$$C_{ps} = \frac{C_{vs}}{\rho_s} = 1419 \; J/kgK. \tag{11}$$

in which ρ_s and ρ_w are the density of soil (1700 kg/m^3) and water (1000 kg/m^3) respectively, w is the water content (15%) and C_{vw} is the heat capacity at constant volume for water which is taken to be 4300 kJ/(m^3·k) (Suomen Rakennusinsinöörien Liitto RIL ry, 2013). The thermal conductivity is assumed to be 1.5 W/(m·K) but will be varied during the parameter sweeps.

The heat flux boundary describing the convective heat losses to the air is relocated to the top of the soil layer, and the inner and outer sides of the soil layer are set to an adiabatic boundary.
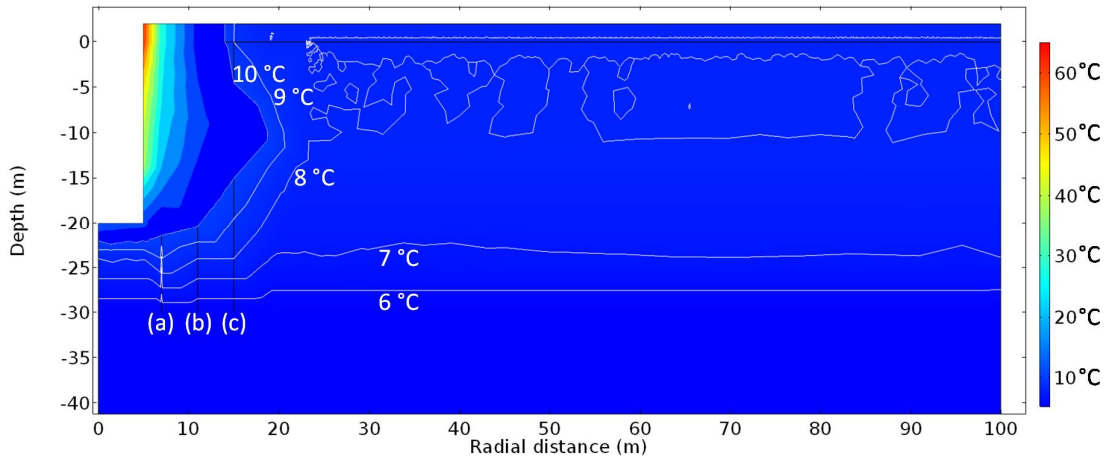
Figure 18. Initial temperature distribution showing the effect of the coarse data and the constant extrapolation with a, b, and c being the constant temperature boundaries at a distance of 2, 6, and 10 m from water store. Soil thickness is 2 m

For the initial temperature inside the domain, an interpolation function is used. It interpolates linear and extrapolates constant. Thus the addition of a soil layer on top of the interpolated domain will attain the same value as for the top of the granite layer (Figure 18). This is too hot and not representing reality, but there is no data on this domain, so to get a temperature distribution that resembles reality better, a study step is introduced that precedes the main simulation step and tries to approach the real values outside the known values. The main simulation, which is the second step, will then use the results of the first

step as its initial values. The initial temperature from Table 3 is split into separate tables, one for each distance from the water store. The temperatures at 2, 6, and 10 m are loaded separately into COMSOL using interpolation functions. Temperature boundaries (a, b, and c in Figure 18) are created at each of those distances, and the temperature is set to its corresponding interpolation function. One other temperature boundary is created that sets the water store boundary temperature to the value of the first day used for the simulation. The heat flux boundary describing the outside air is given an external temperature averaging the 30 days previous to the period of interest which is 10 °C.

Figure 19 shows the result when a stationary study step is used and the isotherms 6 till 10 indicate the problem with a stationary study step in its current setup. The real system is not in equilibrium, but the stationary study step will redistribute the temperatures to obtain the lowest temperature gradients possible to reach equilibrium. This problem can be solved by implementing an additional temperature boundary, specifically to set the temperature at a depth of 30 m to 5.3 °C.
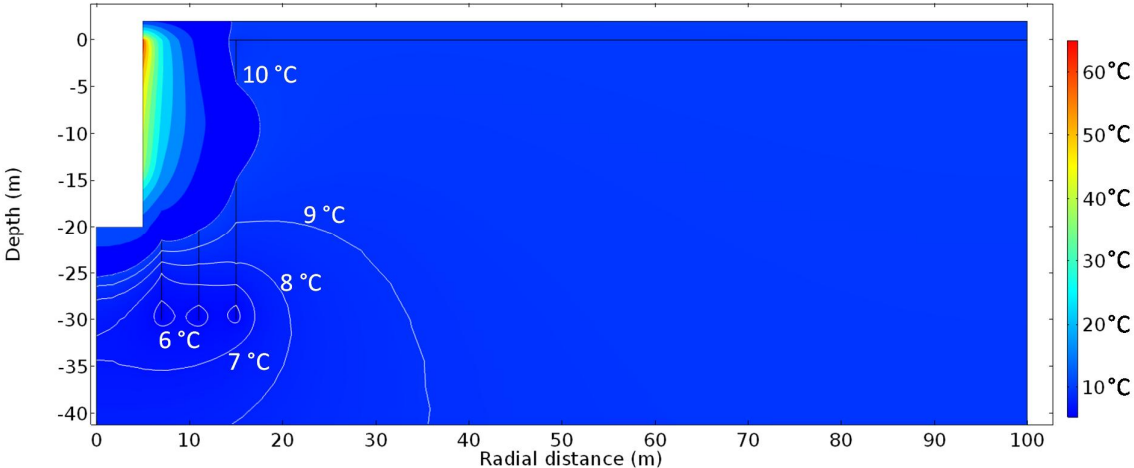
Figure 19. Isotherms after stationary study step with 2 m soil

This additional temperature boundary confines the area in which the temperatures can smooth out. Figure 20 shows that the temperatures are distributed more realistically after the stationary study step and have created a natural temperature gradient outside the water store's influence.
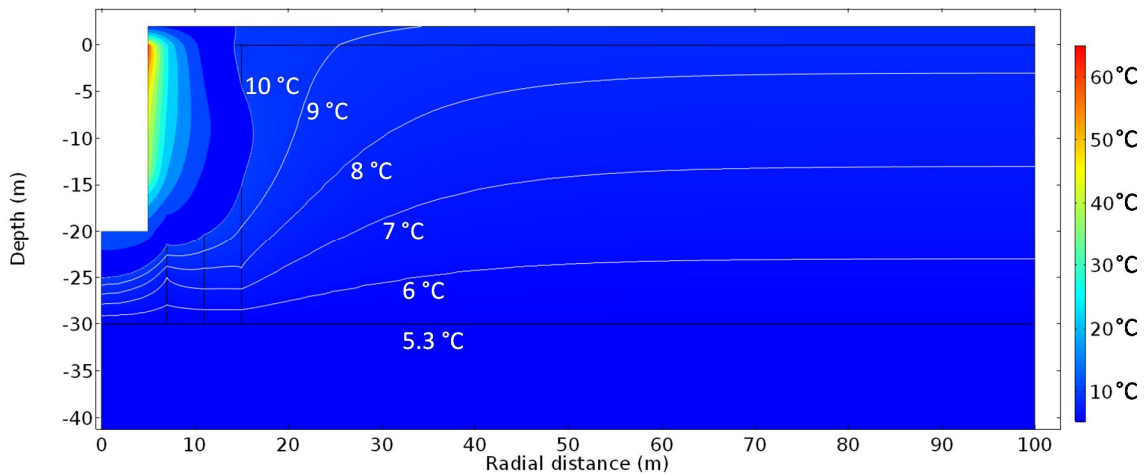
Figure 20. Isotherms after stationary study step including the 5.3 °C temperature boundary at 30 m depth with 2 m soil

With the model set up, the Livelink between COMSOL and MATLAB is used to run the soil thickness parameter sweep and to extract the cut line dataset for plotting the isotherms. For this, the model is loaded into MATLAB, and a for-loop is used to set the soil thickness, run the model, and save it. The cut line data set is exported, and the depths of the isotherms are calculated. The soil thickness parameter is varied between 0.5 m and 7.5 m with increments of 0.5 m.

3.4.1 Results of soil simulation

For a thickness of 0.5, 2, 4 and 7 m the resulting isotherms are plotted in (Figure 21), and as seen, the differences are small with changing soil thickness regarding the isotherms up to and including 30 °C. The 35 °C isotherm does change substantially as expected. The soil is acting as an insulation layer and with increasing thickness, the granite heats up faster as less heat is lost to the environment.
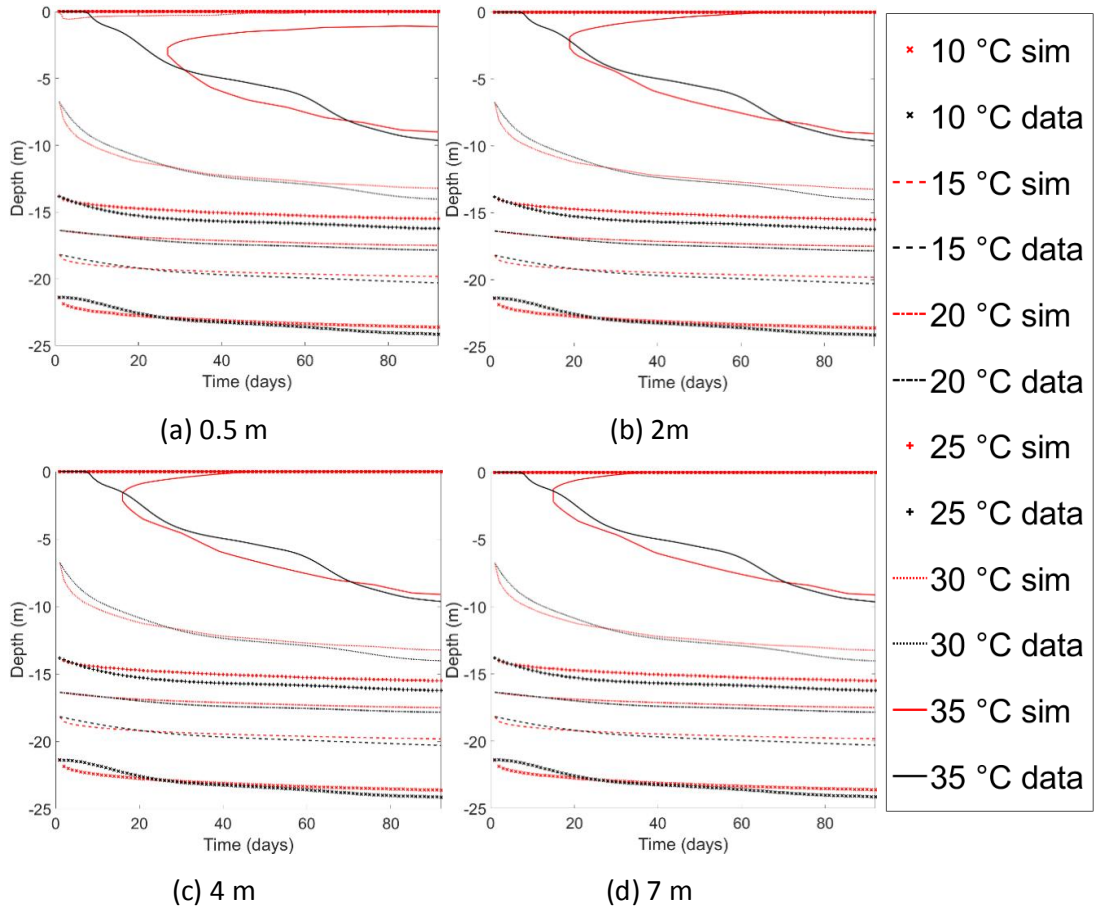
Figure 21. Isotherms with soil thicknesses of 0.5 m (top left), 2 m (top right), 4 m (bottom left), and 7 m (bottom right)

To be able to evaluate which simulation produces better results, a quantifiable parameter needs to be created that represents the quality of historical data reproduction. An obvious parameter would be the coefficient of determination (R^2). As the only isotherm that shows some real change with differing soil thickness is the isotherm 35 °C, this is a good line to use for the determination of the R^2. The problem, however, is that the curve folds back on itself and does not match the same time range as the historical isotherm. This means that the R^2 value needs to be adjusted. The standard R^2 value is calculated for the lower part of the simulated isotherm that shares the time range with the historical one. It is defined as:

$$R^2 = 1 - \frac{SS_{res}}{SS_{tot}}. \tag{12}$$

$$SS_{res} = \sum_t (h_t - s_t)^2 \tag{13}$$

$$SS_{tot} = \sum_t (h_t - \bar{h})^2 \tag{14}$$

43

$$\bar{h} = \frac{1}{n} \sum_{t=1}^{n} h_t \tag{15}$$

Where h_t is the depth of the historic isotherm at time t, and s_t the depth of the simulated isotherm at time t. Then to adjust for the back folding of the isotherm and the part of the historic isotherm that is outside the simulated time range, a surface calculation is done to serve as a penalty to the standard R^2 (Figure 22).
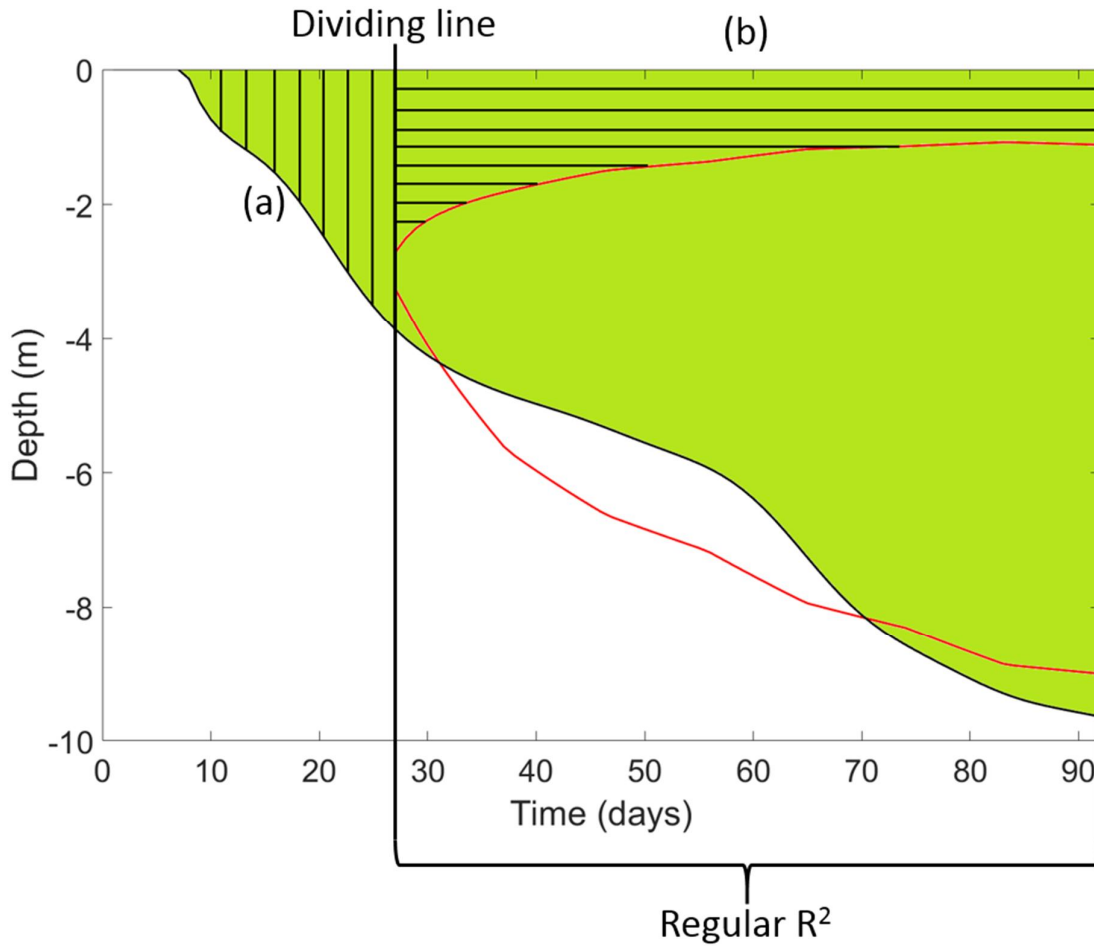
Figure 22. Surface penalty calculation method. The red curve is the simulated 35 °C isotherm, and the black curve is the historic isotherm. Surface (a) above historical curve until the dividing line, surface (b) above the simulated curve from the dividing line and the total green surface above the historic curve (Soil thickness 3 m)

The surface penalty is calculated as a ratio of the mismatch surface to the total green surface above the historic isotherm (Figure 22). The mismatch surface is the surface above the historic isotherm until the dividing line (Figure 22, a) plus the surface above the simulated isotherm from the dividing line (Figure 22, b). This ratio is subtracted from the regular R^2 to give the adjusted R^2 value. The result of this adjusted R^2 calculation is shown in Figure 23 for all simulations.

44
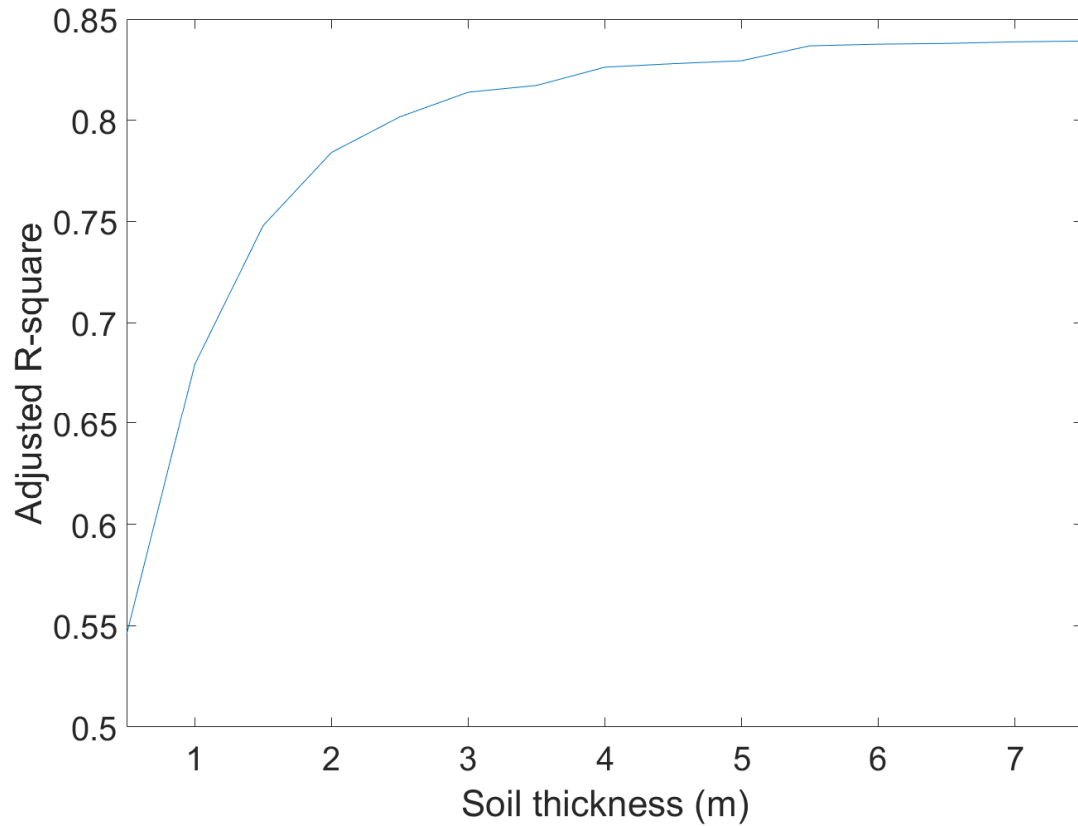
Figure 23. Adjusted R-square values for different soil thicknesses

A second method of quantifying the quality of historical data reproduction has been used to verify the results. For this method, the area enclosed by the two isotherms and/or the axis is marked red, using Microsoft Paint (Figure 24). The resulting image is saved as a .png, 420 by 560 pixels big, and loaded into MATLAB which then counts the number of reddish pixels. A pixel is classified as reddish using the RGB-code (red>180, green<60 and blue<60). The lower the amount of reddish pixels, the better the fit (Figure 25).
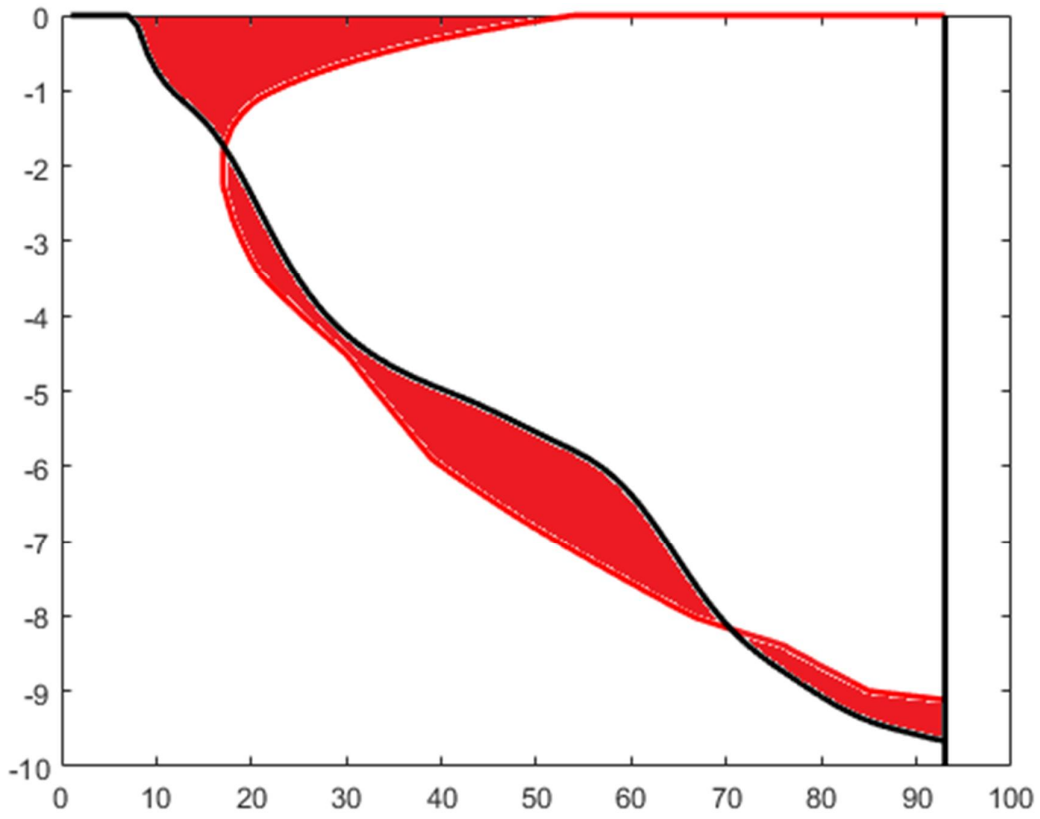
Figure 24. Second method of quantifying the quality of historical data reproduction by counting the number of reddish pixels. (Soil thickness 3 m)
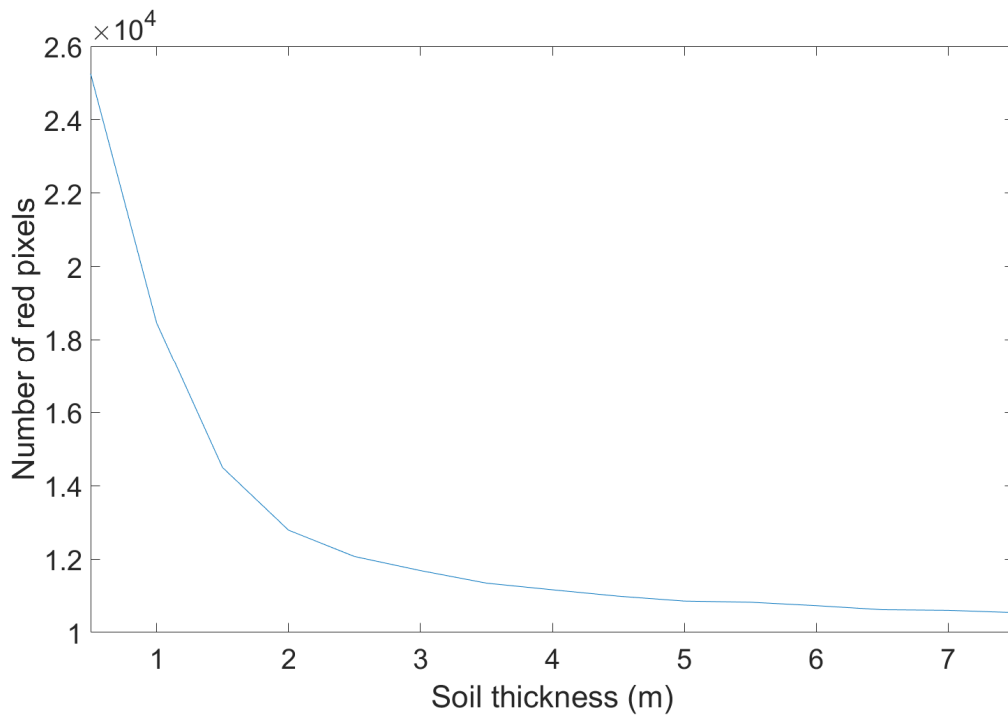
Figure 25. Total number of red pixels describing the area between isotherms and/or axis

3.4.2 Discussion of soil simulation

The lower isotherms are too deep to be influenced by the soil as the granite itself acts as insulation. The two different ways of quantifying the quality of the fit of the 35 °C isotherm, both show that when the soil gets to 4 m in thickness and above the fit does not improve significantly. This is constrained by the thermal conductivity of the soil. When the soil is over 4 m deep the temperature of the surrounding air does not penetrate deep enough anymore to decrease the temperature of the granite. The soil now starts to act as a heat sink in which the heat generated by the water store can escape. So a possible improvement is to reduce the thermal conductivity of the soil to act more like an insulator and less as a heat sink.
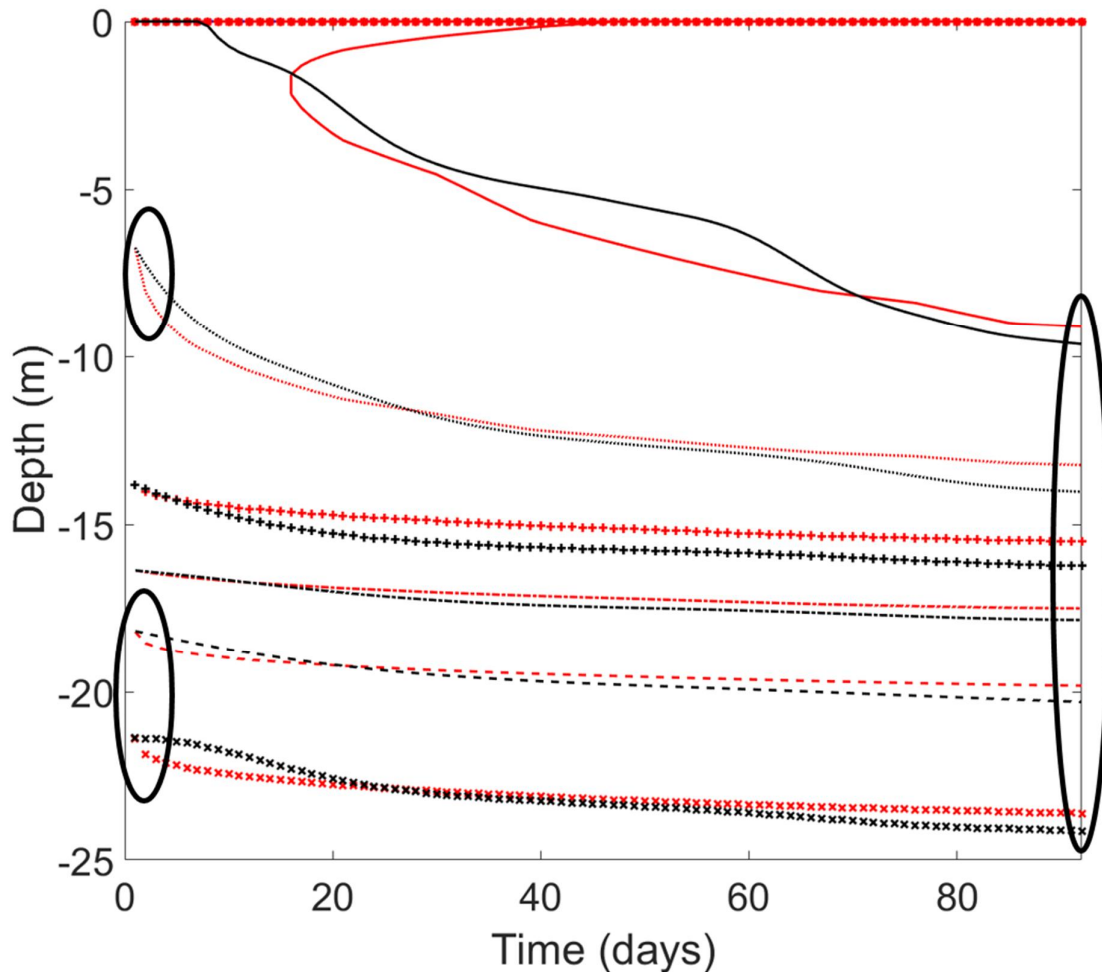
Figure 26. Isotherms with soil thickness of 4 m, showing the inconsistencies between the simulated and historical data. Encircled areas on the left show the faster decrease in depth of the simulated isotherms compared to the historical ones, Area on the right shows the difference in final depth

Figure 26 highlights the inconsistencies between the simulated and historical isotherms. The first major difference is the fast increase in depth of the simulated isotherms in the early stage of the simulation. This can be explained by the way the initial temperature

distribution is modeled in the first study step (Figure 20). The temperature is set on the known boundaries but free to change in between and thus creates waves in the isotherms. These will straighten out quickly at the beginning of the second study step. The second inconsistency in Figure 26 on the right is the final depth of the simulated isotherms. An explanation for this can be that the used thermal conductivity for granite is too low.

3.5 *Parameter sweep using the 2D model*

As discussed previously, the thermal conductivity of the soil might be too high and the thermal conductivity of the granite too low. To investigate this, both thermal conductivities are used in a parameter sweep. New historical data has surfaced that contains technical drawings of the topography, soil layer and bedrock (SITRA, 1980). Figure 27 shows a plan view of the Kerava site including locations of the water store and five boreholes surrounding it including collar depth, depth of the bedrock and total borehole length. Figure 28 and Figure 29 show the cross-section A-A and B-B respectively. The assumed bedrock profile is drawn in the figures and therefore the soil thickness in the Northern direction, 2 m away from the water store, is taken to be 4 m and implemented in the 2D-model as a uniform horizontal layer.
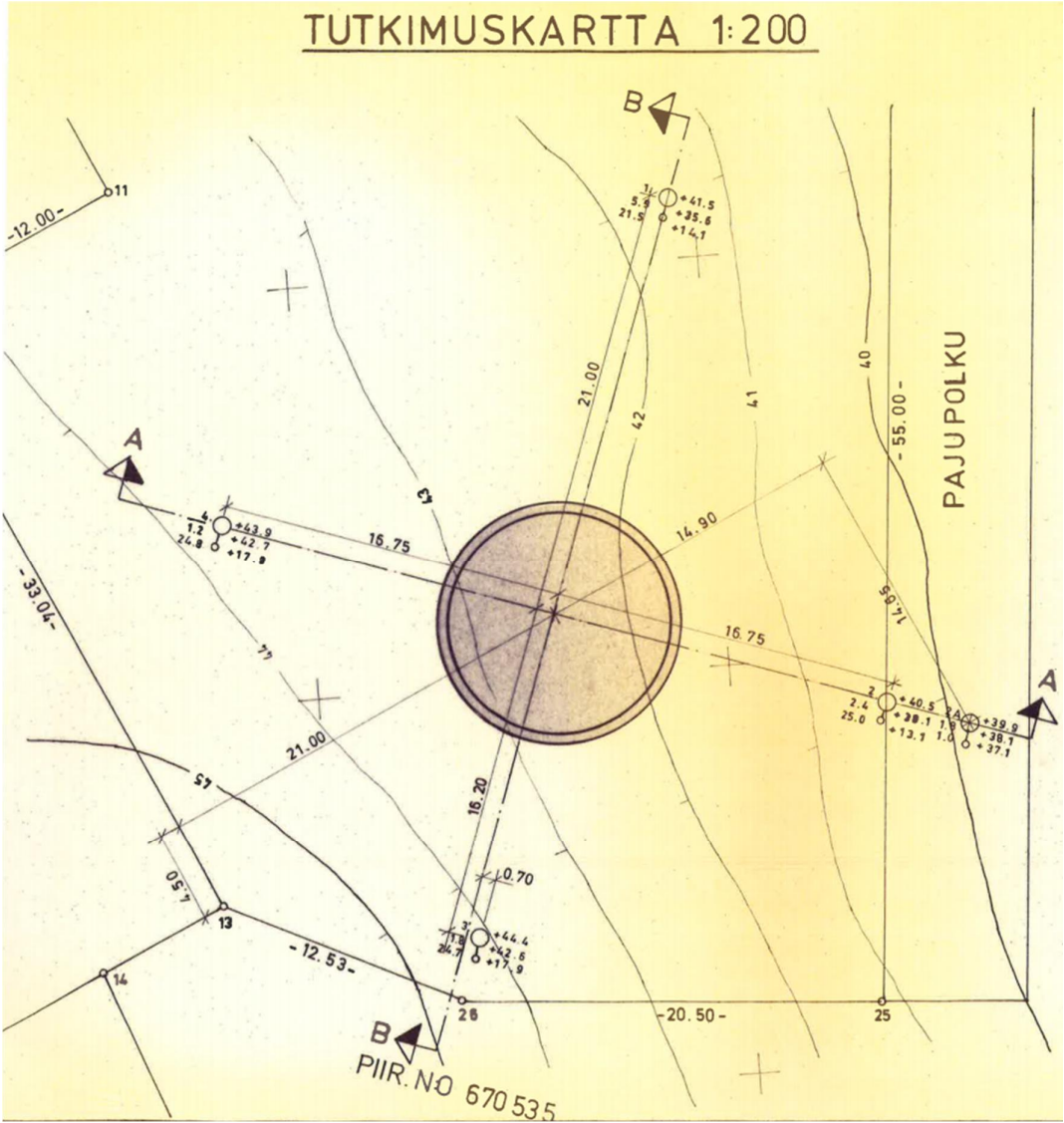
Figure 27. Plan view of Kerava site with the location of drill holes and the water store
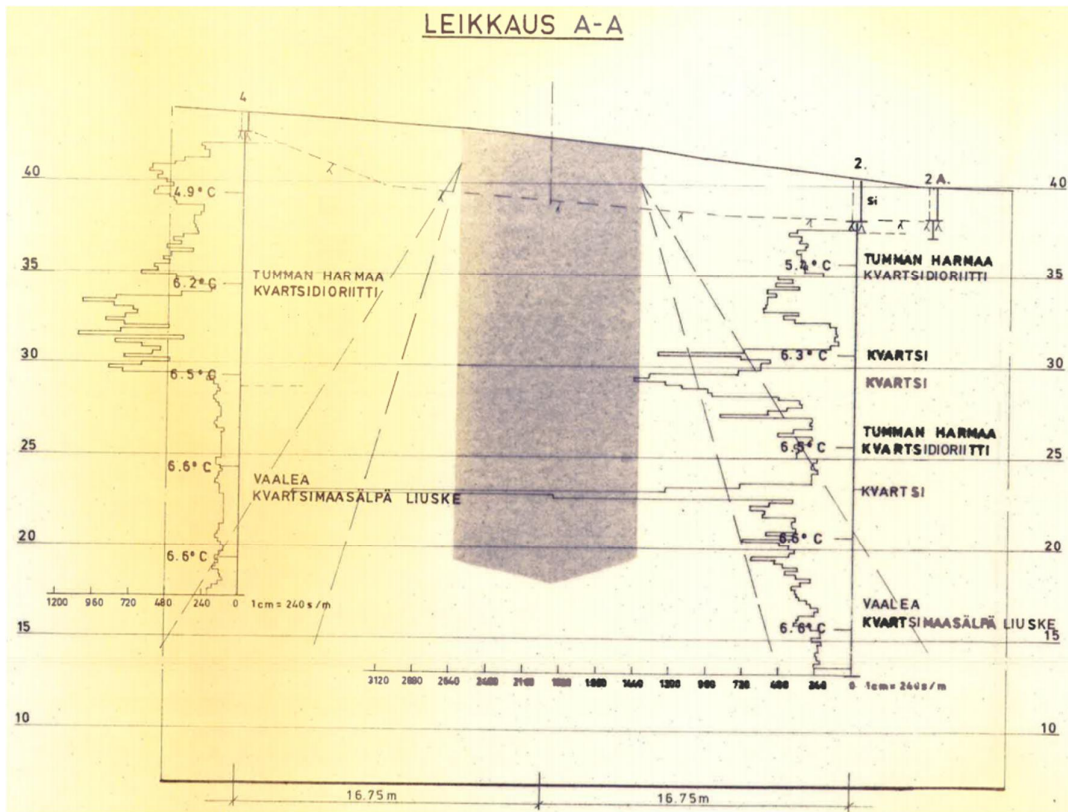
Figure 28. Cross-section A-A including data on the soil and rock types plus elevations
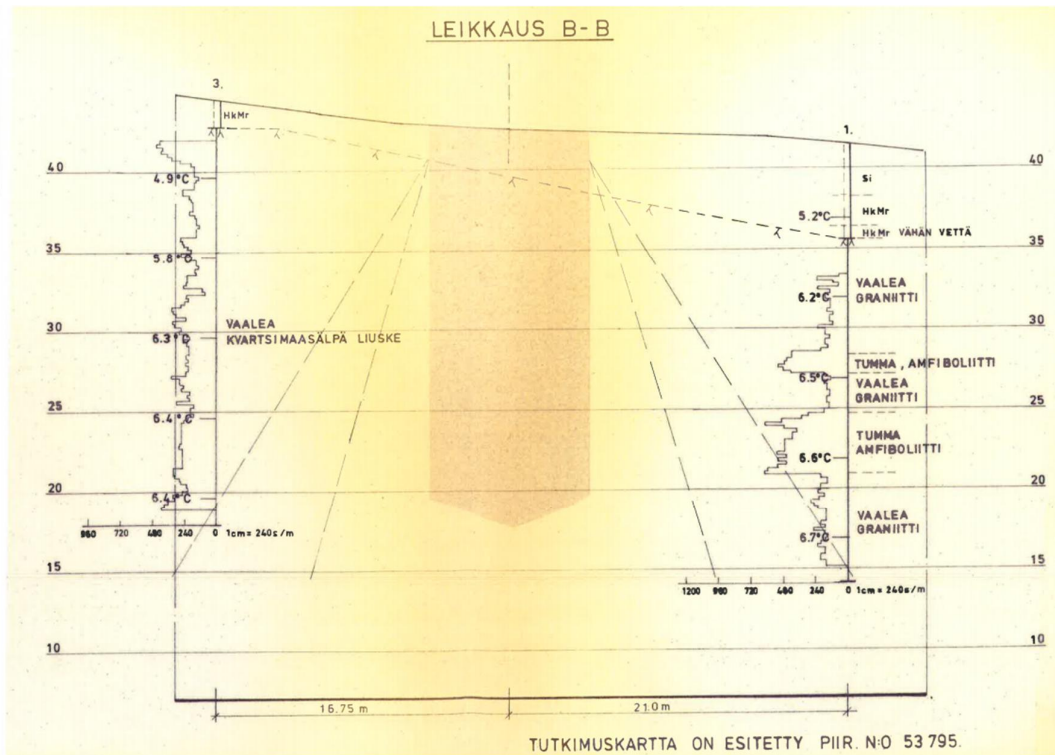
Figure 29. Cross-section B-B including data on the soil and rock types plus elevations

With the soil thickness set to 4 m, the thermal conductivities are varied. According to the SITRA (1980) document, the soil thermal conductivity was between 1 and 2 W/(m·K) and for the granite between 3 and 4 W/(m·K) and so they both will be varied with increments of 0.2 W/(m·K) creating 36 separate simulations.

3.5.1 Results and discussion of parameter sweep

As in the soil thickness simulation, a quantifiable parameter needs to be created. Because the thermal conductivity of the granite will be varied this time, the isotherms at depth will be changing as well and thus will need to be incorporated in the R-square method. An R-square value is calculated for each isotherm, and they are added together and divided by six to create an average R-square value.
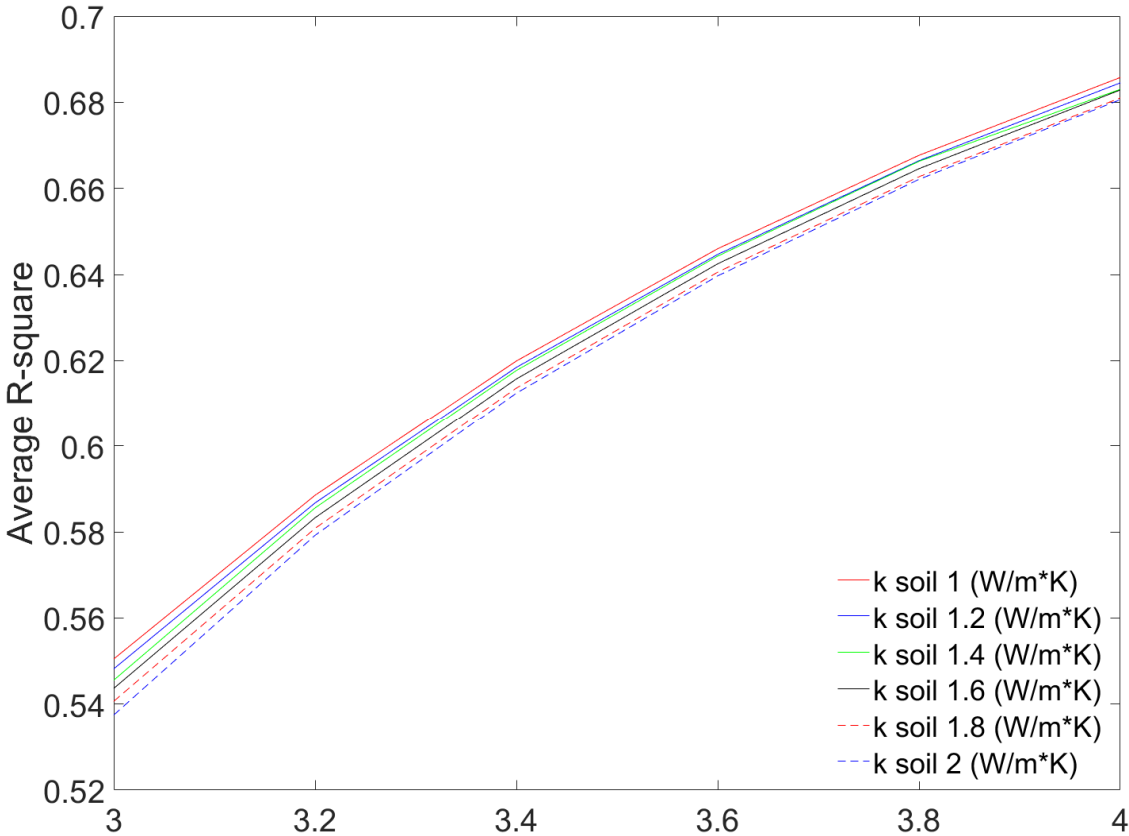
Figure 30. Average R-square for different thermal conductivities of granite and soil using the 2D model

Figure 30 shows the result of these simulations and as seen the influence of the soil conductivity is much lower than for the granite. This, however, is because the soil conductivity only has an impact on the 35 °C isotherm and the thermal conductivity of granite has an influence on all the isotherms. For this reason, the R-square for the 35 °C isotherm is calculated separately with a varying conductivity for the soil and granite within their respective ranges (1-2 W/(m·K) for soil and 3-4 W/(m·K) for granite).
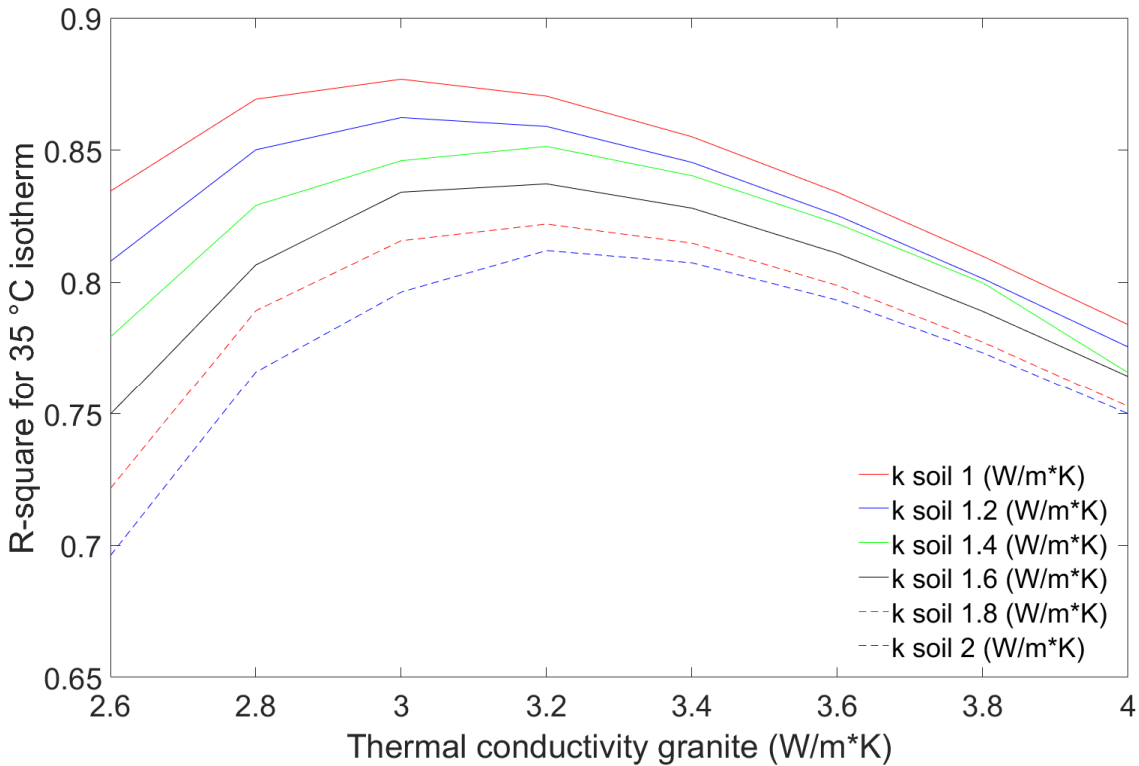
Figure 31. R-square values for the 35 °C isotherm with lowered conductivity for granite to find the optimum using the 2D model

As seen in Figure 31, the optimum within the realistic ranges of conductivities is at 1.0 W/(m·K) for the soil and 3.0 W/(m·K) for the granite. Figure 31 is showing a larger range for the conductivity of granite to show the optimum. The simulation with soil and granite conductivity of 1 and 4 W/(m·K) respectively, produced the 40 °C isotherm at the end of the simulation.

A short investigation showed, that with an increasing conductivity of the granite past the realistic range with the soil conductivity set to 1 W/(m·K), the 40 °C isotherm shows up as well. The same goes for a decreasing soil conductivity with the granite conductivity set to 4 W/(m·K) and according to the historical data the 40 °C isotherm should not show up, and therefore, the conductivity ranges are limited on the high end of the granite conductivity range.

Figure 30 shows that with an increasing thermal conductivity of granite, the R-square of all isotherms combined increases regardless of the decreasing fit for the 35 °C isotherm shown in Figure 31. To increase the fit of the lower isotherms, the conductivity of the granite needs to be increased. Figure 32 shows the average R-square for increasing the conductivity of granite for all isotherms in black and for all isotherms except the 35 °C isotherm in red. For all isotherms, the optimum is around 5.5 W/(m·K), and for all isotherms except the 35 °C, it is around 7 W/(m·K). However, as mentioned before, the 40 °C isotherm shows up in all of them and therefore these values are not allowed, besides the fact that they are outside the realistic range.
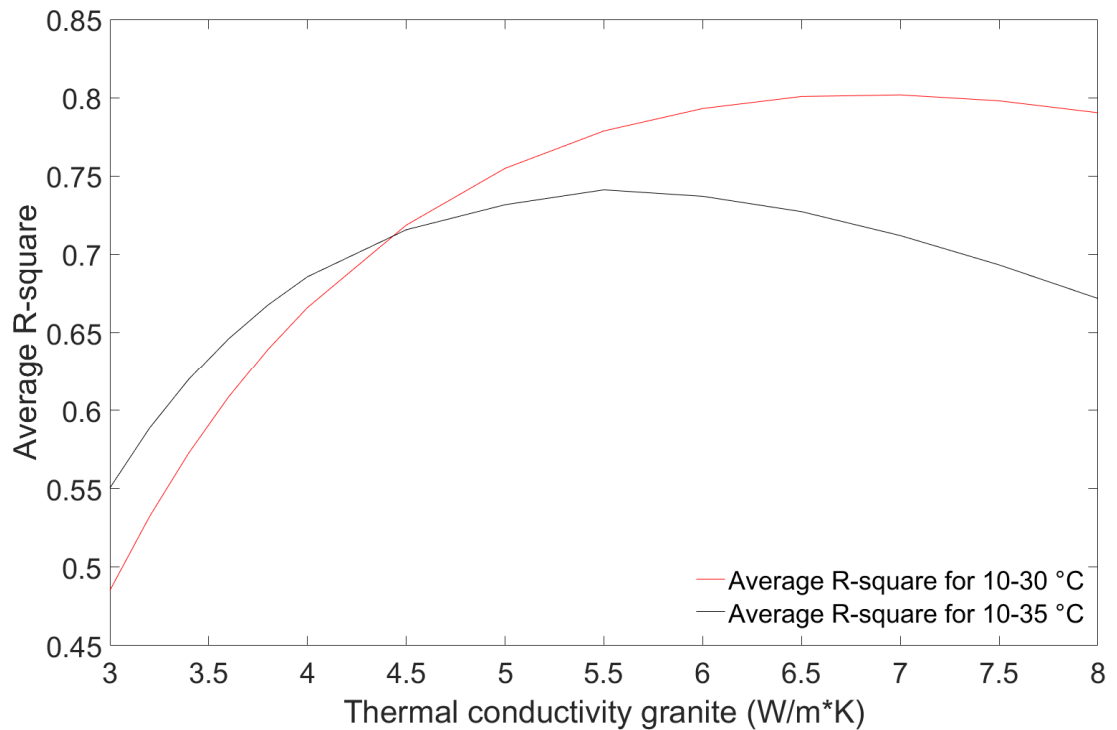
Figure 32. Average R-square for the isotherms 10 until 30 °C (red) and 10 until 35 °C (black) with soil conductivity of 1.0 W/(m·K), using 2D-model

3.6 *The 3D-model*

The previous model was a 2D-axisymmetric model and thus only an approximation. The topography was modeled as a flat surface, and the soil was a uniform layer of 4 m in thickness. Using the dimensions given in Figure 27, Figure 28, and Figure 29 a 3D model was created in AutoCAD. Soil and granite layers are created according to the drill data from Figure 28 and Figure 29.

In the B-B cross-section, there is a Sandy Moraine layer present, but this is disregarded in the model as the thermal properties are similar. The same goes for the bed-rock which is modeled as a single layer of granite.

Both models are made up out of concentric domains with the fist domain being a cylinder with 7 m radius (blue), the second a hollow cylinder with inner radius of 7 m and outer radius of 11 m (magenta), the third with radii 11 m to 15 m (green), the forth from 15 m to 19 m (yellow), and the last from inner radius of 19 m to a square of 100 m (red) (Figure 33). These concentric domains are created to assign the known temperatures to those boundaries during the first time-dependent study to even out the temperature distribution inside the unknown temperature space.

53
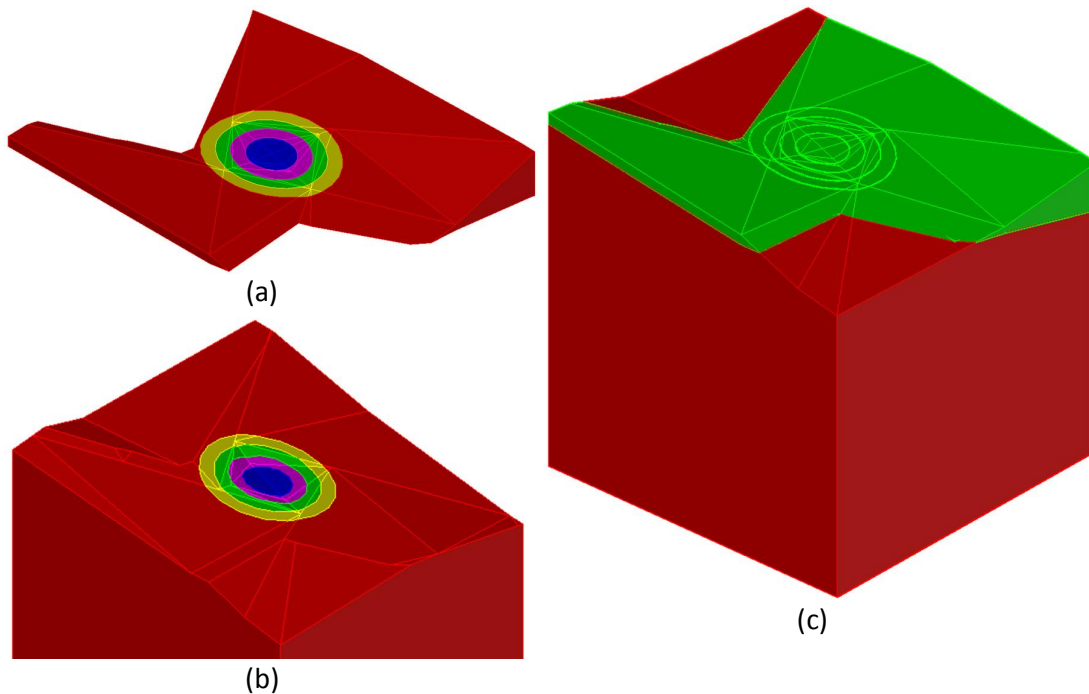
Figure 33. 3D-Models from AutoCAD according to the technical drawings of Figure 27, Figure 28, and Figure 29, with (a) soil layer, (b) bedrock and (c) assembly of soil and bedrock. Blue is inner cylinder of radius 7 m, magenta is 7 m until 11 m, green is 11 m until 15 m, yellow is 15 m until 19 m, and red is 19 m until border

When looking at the drawn-in water store in Figure 28 and Figure 29, and knowing its height was 20 m, it is assumed that the water level is at elevation 40 m. To make everything easier in COMSOL, all coordinates in the model are changed with regards to their Z-values to match the water level to a Z-value of zero.

With the geometry imported, the water store is created and cut out of the model. Two work planes are used, on the XY-plane with a Z-value of 0 and -30 m, to draw circles with radii of 7, 11, and 15 m to create edges on the different domains, dividing their surfaces. These divisions are needed to assign the known temperature distributions to the correct surfaces and depths. Also, one circle is drawn at elevation zero to mark the water level.

The same material properties are assigned to the domains as for the soil simulations with the conductivities as parameters to be varied.

A two-step study is used again in which the first step is to even out the temperatures that are passed through to the next step as initial values. Table 4 shows a list of all boundary conditions used for each step which is visualized in Figure 34.

Table 4. List of boundary conditions used in each study step

First stationary study step		
Type of boundary	**Surface shown in Figure 34**	**Description**
Heat flux boundary	On the top surface. (green line)	Modeling the heat flow due to the outside air. Temperature set to the average of the 30 days previous to the simulation which was 10 °C
Temperature Boundary	5 m cylinder of height 20 m. (red line nr. 1)	Temperature distribution of the water store on the first day
	7 m cylinder of height 30 m. (red line nr. 2)	Initial temperature distribution of the rock 2 m from water store
	11 m cylinder of height 30 m. (red line nr. 3)	Initial temperature distribution of the rock 6 m from water store
	15 m cylinder of height 30 m. (red line nr. 4)	Initial temperature distribution of the rock 10 m from water store
	XY-plane with elevation -30 m. (red line nr. 5)	Set temperature at depth of 5.3 °C
Thermal Insulation	Part of the water store above the water line. (blue line)	Assuming that the structure above the water line is well insulated
	Sides and bottom of the model. (blue line)	Model dimension is taken big enough to avoid contamination of the results
Second, time-dependent, study step		
Type of boundary	**Surface shown in Figure 34**	**Description**
Heat flux boundary	On the top surface. (green line)	Modeling the heat flow due to the outside air
Temperature Boundary	5 m cylinder of height 20 m. (red line nr. 1)	Temperature distribution of the water store
Thermal Insulation	Part of the water store above the water line. (blue line)	Same as the first step
	Sides and bottom of the model. (blue line)	Same as the first step
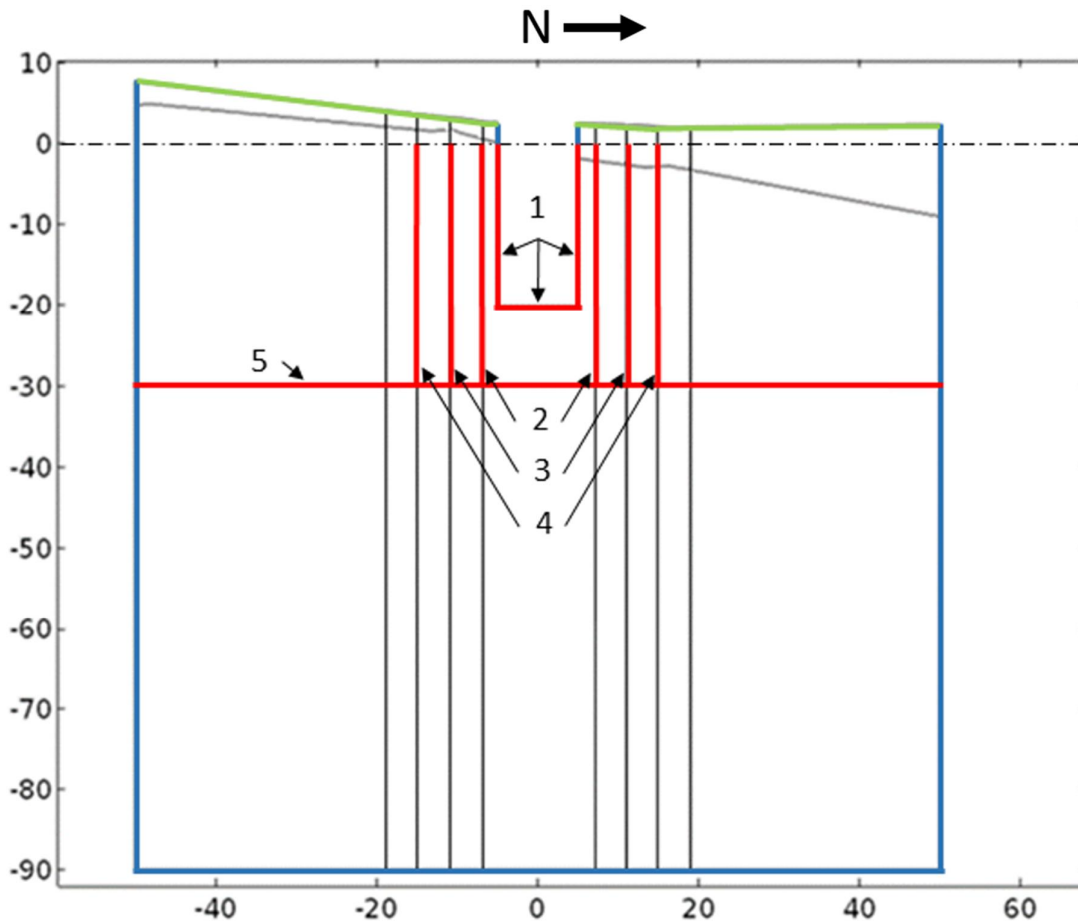
Figure 34. North-South Cross-section of the 3D-model. Red lines show the location of temperature boundaries with 1 for the water store, 2-4 for the concentric cylinders (radii of 7, 11 and 15 m) with known temperatures, and 5 for the low temperature at depth. The green line shows the heat flux boundary at the top surface, and blue show the insulated boundaries on the outside of the model and in the water store above the water line

Just as for the 2D simulation, the outside air temperature, the water store temperature, and the initial rock temperature are imported using the interpolation function in the global definitions tab. The initial rock temperature table had to be changed from a 2D table (x and z) to a 3D table (x,y and z). To set the temperatures to the concentric cylinders, four more interpolation functions (one for the water store and three for the cylinders inside the rock) are used to describe the temperatures relative to their depth.

The required precision level of the simulated results is decreasing with increasing distance from the water store, and thus the mesh can get coarser with increasing radius and depth. The domain that is directly surrounding the water store uses the predefined extremely fine element size and the concentric domains going outward will get the predefined extra fine, finer, and the fine element size. The last one is slightly customized to use a minimum element size of 1.06 m to avoid problems with narrow regions. The domains below a depth of 30 m and the domain surrounding the last cylindrical domain will get the predefined normal element size. These regions are shown in Figure 35.
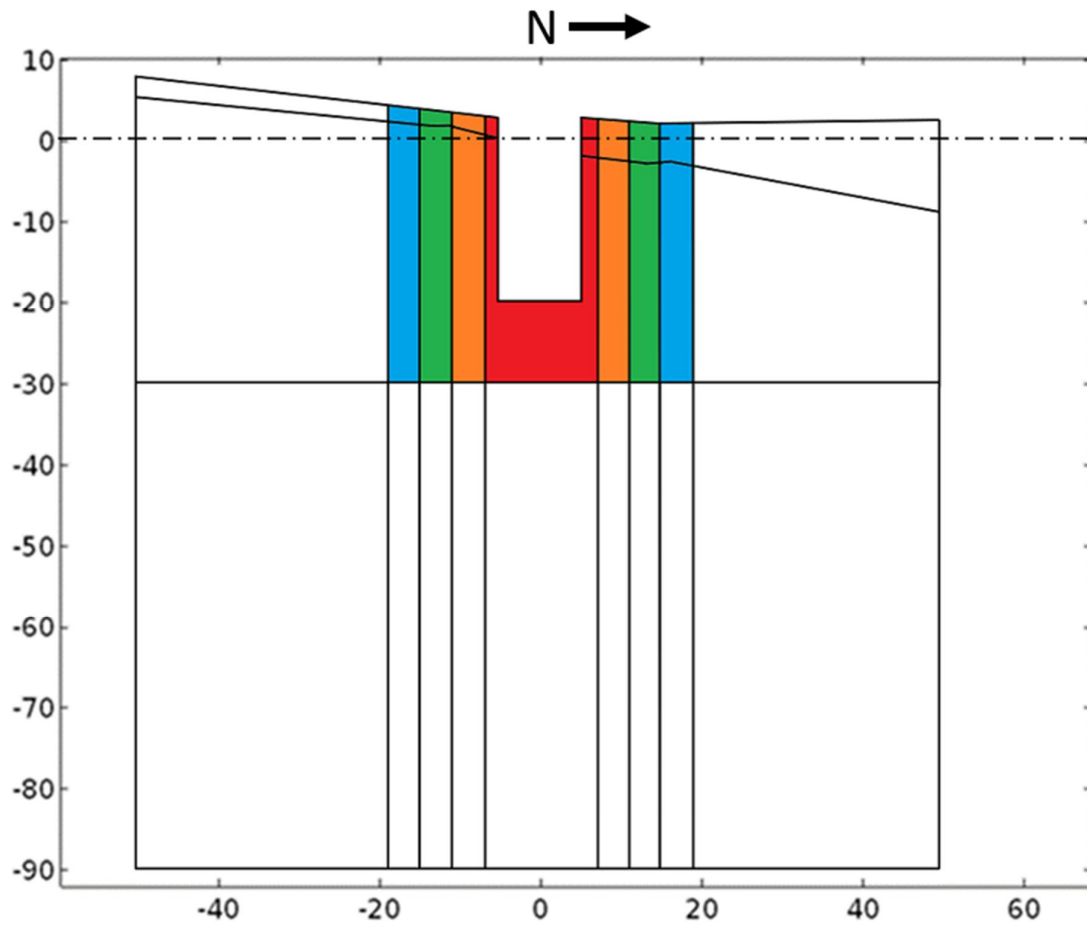
Figure 35. North-South cross-section of the model showing the areas of different mesh size. Red: predefined extremely fine, Orange: predefined extra fine, Green: predefined finer, Blue: custom fine with minimum element size = 1.06 m, and white predefined normal size
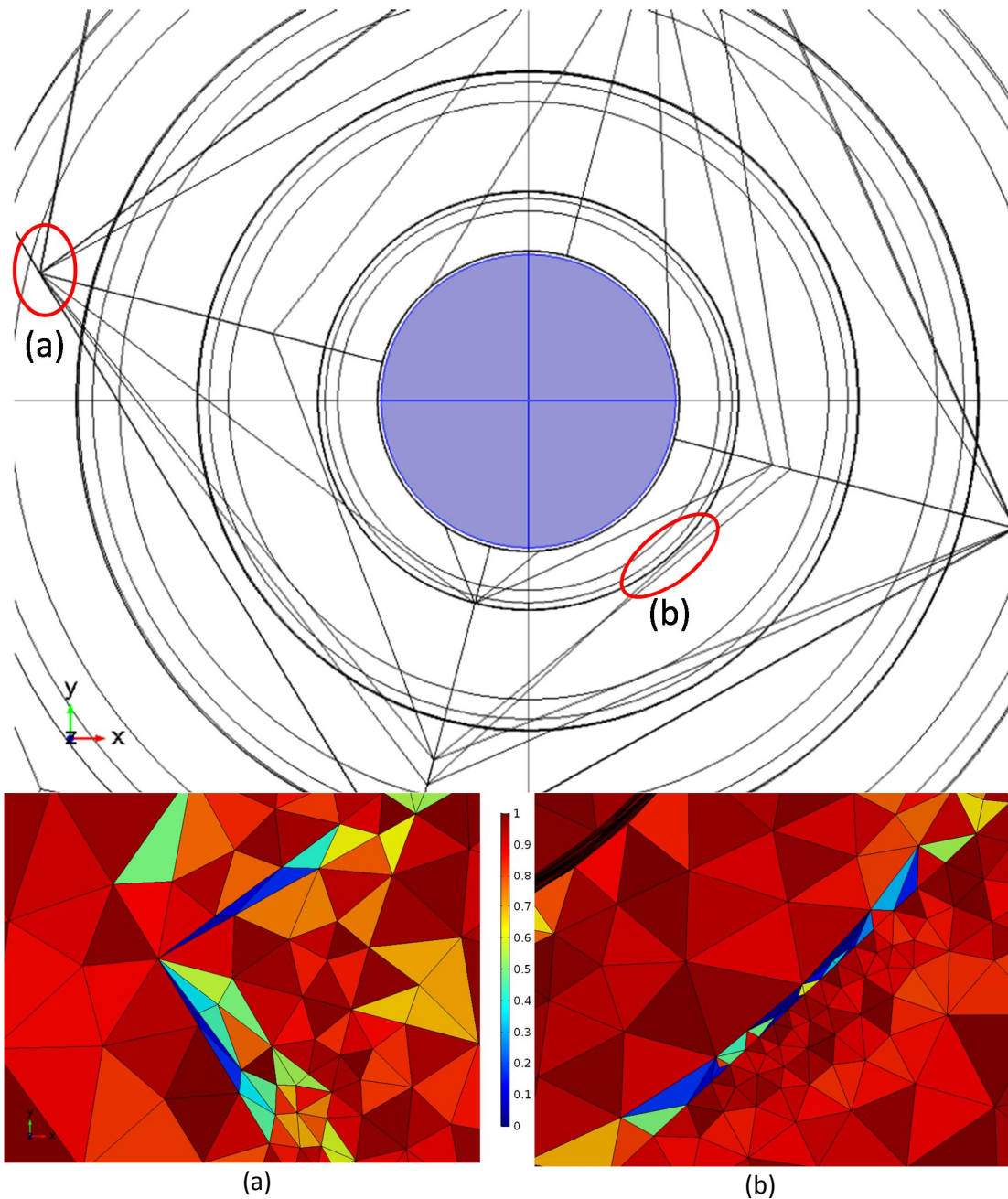
Figure 36. Poorest element areas with (a) and (b) enlarged and plotting their element quality

With the mesh build as discussed previously, there are still some problematic regions as shown in Figure 36. The overall minimum element quality, which is found in Figure 36 (b), is $7.327 \cdot 10^{-12}$ but because they are all in an area that is off low interest this should not interfere with the results. The average element quality of all 230 905 elements is 0.71.

Finally, to be able to compare the simulated results to the historic data, the same cut-line dataset is created at a distance of 2 m from the water store in a northern direction with a depth of 30 m. Along this cut-line, 300 elements are distributed to increase the accuracy.

3.6.1 Results and discussion

The thermal conductivity of the soil and the granite are varied again within their realistic ranges of 1-2 and 3-4 W/(m·K) for soil and granite respectively with increments of 0.2 W/(m·K) for each. The resulting data from the cut-line is exported, and the same algorithm as for the parameter sweep for the 2D model is used to calculate the average R-square for all isotherms, as shown in Figure 37.
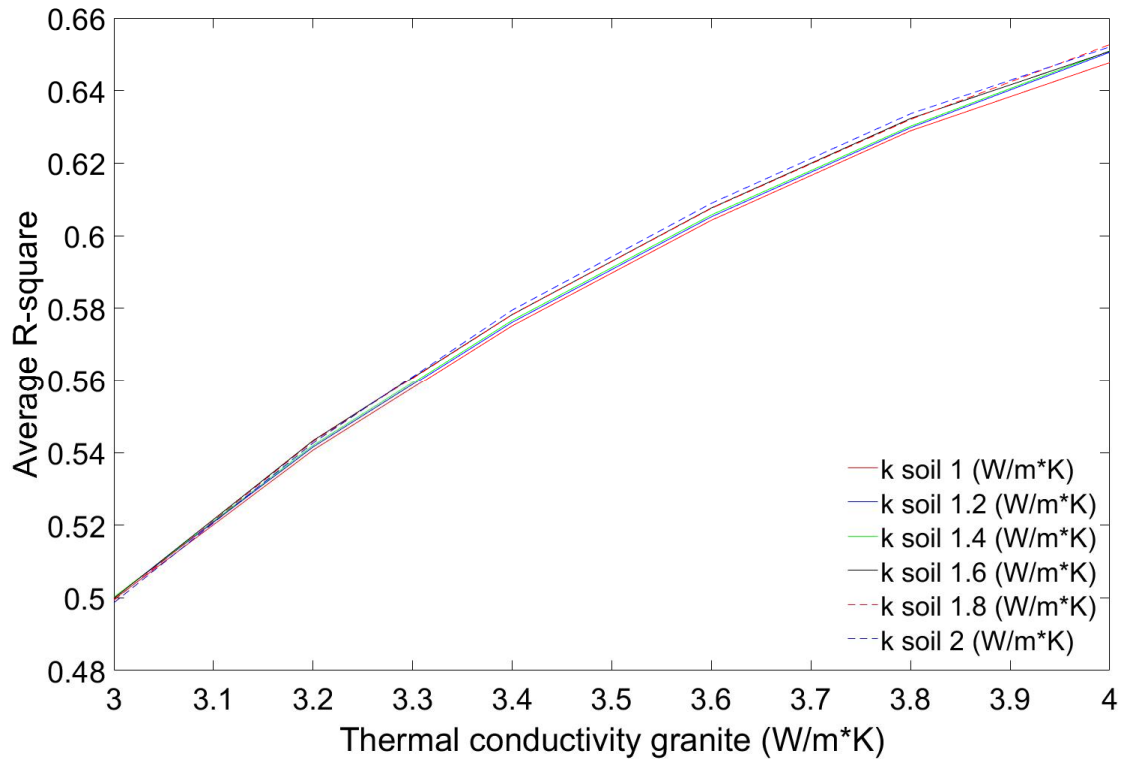
Figure 37. Average R-square for different thermal conductivities of granite and soil using the 3D model

When comparing to the results in Figure 30, the main differences are that the higher soil conductivity gives a higher R-square value instead of a lower one, and that with an increasing conductivity of the granite, the influence of the soil conductivity increases. This increase in influence comes from the 35 °C isotherm. Figure 38 shows the R-square values for the 35 °C isotherm only with an increased range of the conductivity of granite to find the optimum.
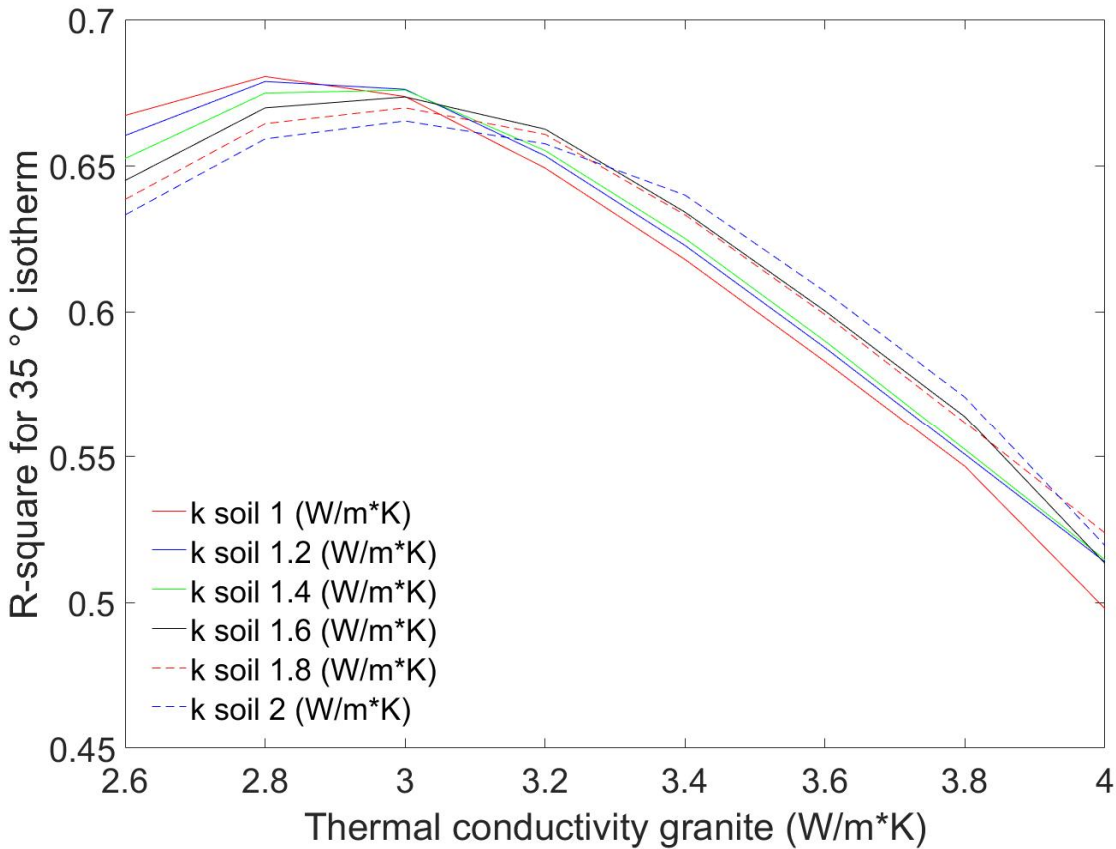
Figure 38. R-square values for the 35 °C isotherm for different thermal conductivities of granite and soil with a lowered range for the conductivity of granite, using the 3D model

With a conductivity of granite of 3.4 W/(m·K) or higher, the higher conductivities of soil give higher R-square values. With a conductivity of granite below 3.4 W/(m·K), the lower conductivities of soil give higher R-square values. It seems that with increasing conductivity of granite the heat is transported too fast, and an increase in soil conductivity can make the soil act more like a heat sink in which some of the heat can escape, improving the R-square. With decreasing conductivity of granite, the heat is not transported fast enough, and a decrease in soil conductivity can serve as extra insulation.

The maximum R-square value is substantially lower than for the 2D model with a 4 m soil layer (Figure 31), from just under 0.88 to just under 0.68 and for a conductivity of 2.8 W/(m·K) for granite and 1.0 W/(m·K) for the soil. This is probably because the water level is inside the soil layer and this is investigated next by lowering the water level by 2 m.

To find the optimum for all isotherms, the conductivity for granite is increased again with a constant soil conductivity of 2 W/(m·K) as that showed the highest R-square value with increasing conductivity for granite (Figure 37). Figure 39 shows the optimum is for a conductivity of 5.5 W/(m·K) when looking at all isotherms (black) and 6.5 W/(m·K) when looking at all except the 35 °C isotherm (red).

60

Figure 39. Average R-square for the isotherms 10 until 30 °C (red) and 10 until 35 °C (black) with soil conductivity of 2.0 W/(m·K), using 3D-model

3.7 *3D-model with lowered water level*

When constructing the rock pit, the soil is excavated down to bedrock so a reasonable assumption would be that the rock pit, as it is drawn in Figure 28 and Figure 29, was actually a little deeper, so the water level was in the rock. For this reason, the model has been adjusted by elevating each domain by 2 m, so the zero level (water level) is about 30 cm below the bedrock, in the northern direction, and the parameter sweep is run again.

3.7.1 Results and discussion

Figure 40 shows the result of the parameter sweep and it can be observed that it is very similar to the parameter sweep of the 2D-simulation shown in Figure 30. The same goes for Figure 41 when looking at the 35 °C isotherm only and comparing it to Figure 31. The maximum R-square is now reached for a conductivity of granite of 2.8 W/(m·K) when looking at the 35 °C isotherm, and is over 0.9 and shows that the lowering of the water level does improve the historical data replication.

Figure 40. Average R-square for different thermal conductivities of granite and soil using the 3D model with the water level lowered by 2 m

To find the optimum for all isotherms, the conductivity of granite is increased again with a constant soil conductivity of 1 W/(m·K). Figure 42 shows the optimum is for a conductivity of 5.5 W/(m·K) when looking at all isotherms (black) and 6.5 W/(m·K) when looking at all except the 35 °C isotherm (red).
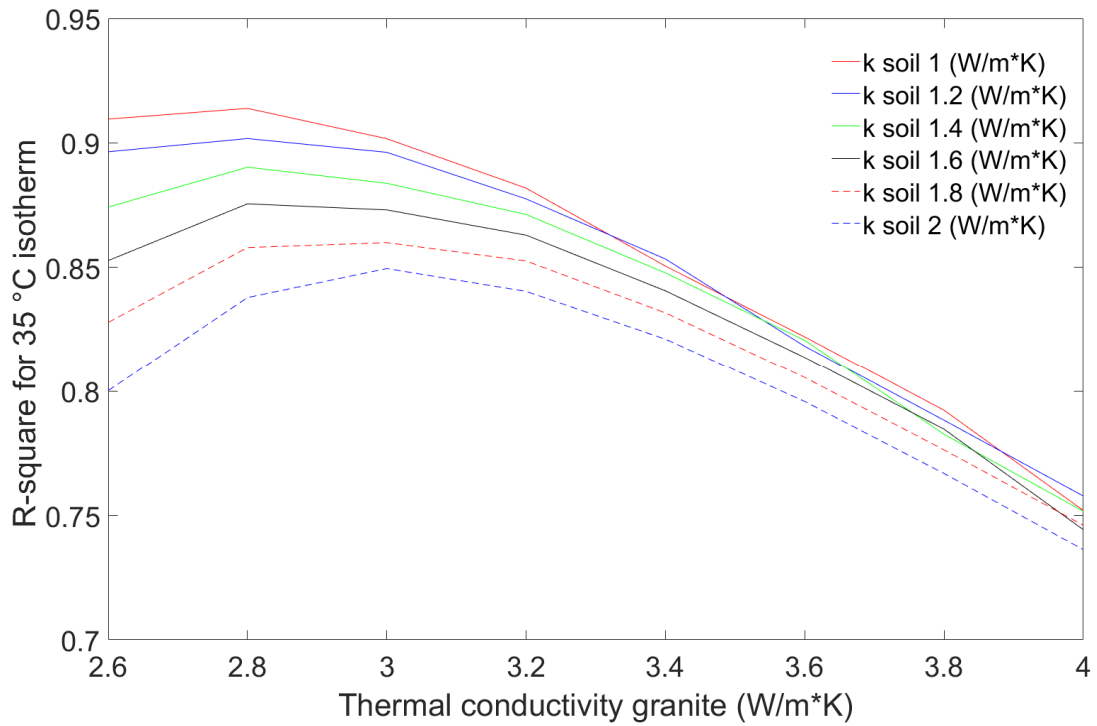
Figure 41. R-square values for the 35 °C isotherm for different thermal conductivities of granite and soil using the 3D model with lowered water level
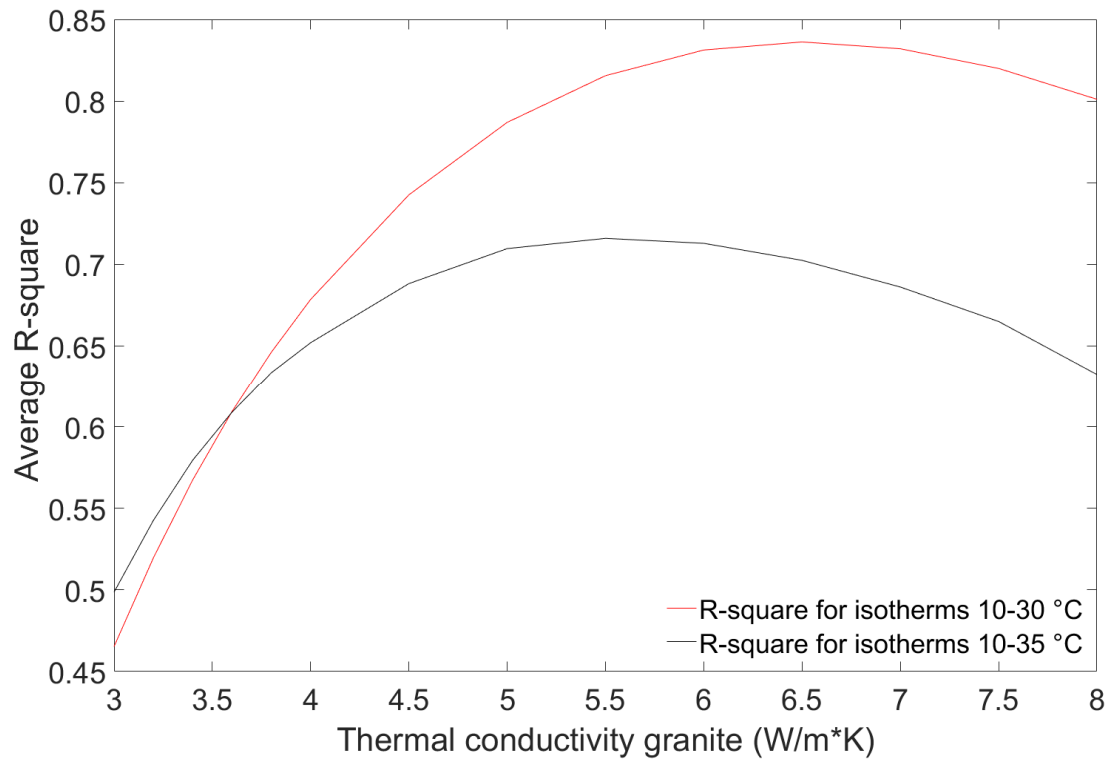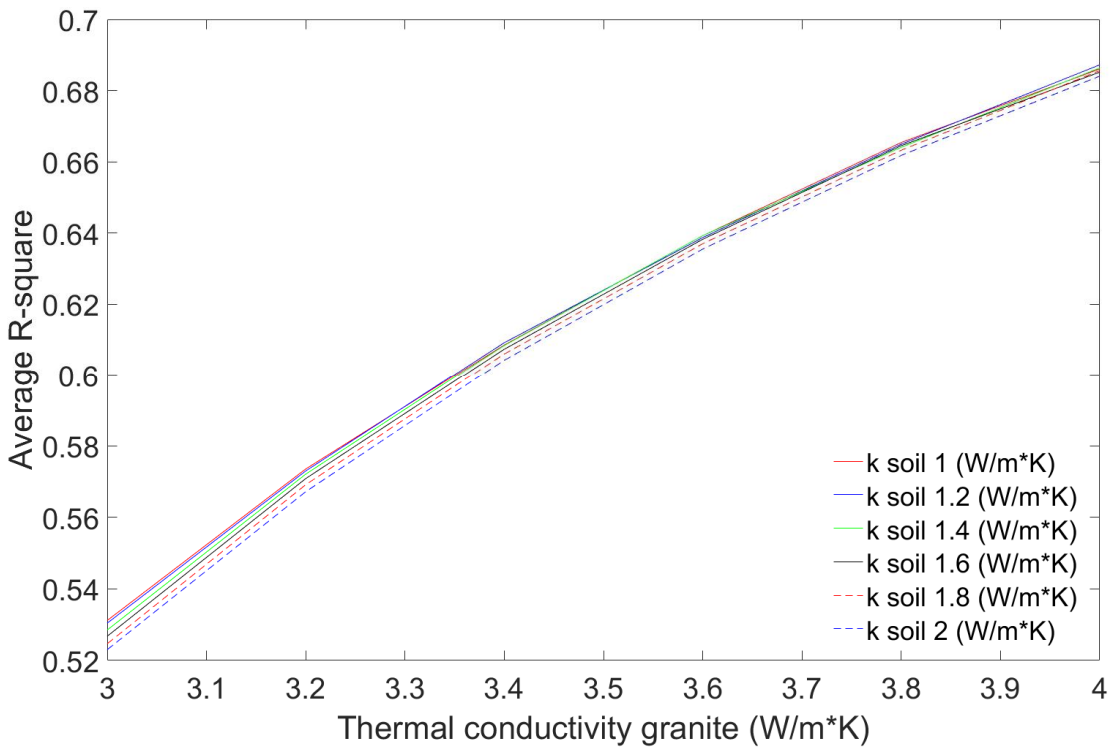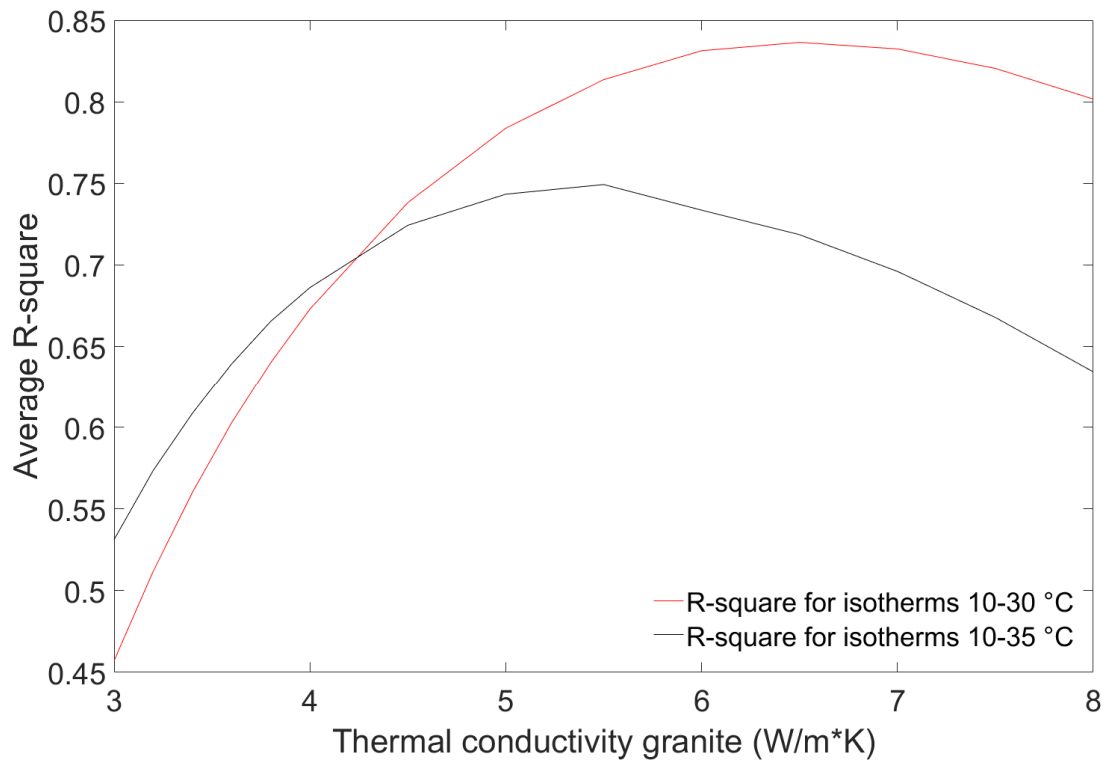

Figure 42. Average R-square for the isotherms 10 until 30 °C (red) and 10 until 35 °C (black) with soil conductivity of 1.0 W/(m·K), using 3D-model with lowered water level

4 Discussion

This chapter discusses the limitations of the created models, as well as provides a summary of the main discussions points that led to each consecutive model.

4.1 *Overall model limitations*

With the limited available data, many assumptions and simplifications had to be made.

The surrounding geology is modeled as one layer of soil and one layer of bedrock. They are given the thermal properties of average Finnish rock and soil as described in Chapter 3.3 and 3.4 for the rock and soil. The only available data on the geology came from 4 boreholes which showed separate layers of soil and bedrock. They do not, however, show consistency. Present layers in one borehole do not show up in the others, and thus it is impossible to create separate layers accurately. Also, the soil and granite layer are both modeled as isotropic materials which they almost never are.

The water store is always modeled as a temperature boundary for which the temperature comes from a graph (Figure 8), depicting isotherms changing in depth over time. The sensors that measured the temperature inside the water store were probably situated in the center of the water store where the temperature will be different than at the water to rock interface. For a more comprehensive model, the water store should have been modeled as a body of water in which there was turbulence, created by the automated winch. Also, according to Lund (personal communication, 1st of June 2016), the water level inside the water store was not always the same because there was some leakage into the surrounding rock. These facts are not implemented into the model because they were not documented.

The temperature distribution in the surrounding rock contains many assumed values. The raw data collected from the Kerava site was destroyed just prior to the start of this research, which contained temperature readings at 2 m, 6 m, 10 m, and 14 m away from the water store and up to a depth of 24 m with one sensor every 3 m. The data used in these simulations for the initial temperature contains only the depth of the isotherms, provided through an interpolated graph of those sensors, and assumed values in between (Table 3). Because the depth of the isotherms is interpolated values between coarse sensor arrays, they will not be very precise (Figure 7).

Because of these shortcomings in the data, the choices for a time window to be used and a method for constructing the model, are limited. That is why the boreholes are left out of the analysis, but to produce a calibrated model that can be used in optimizing the underground thermal energy storage system for the Solar-Community Concept project, the borehole storage is very important.

4.2 *Discussion summary of the individual models*

The cooling down of the surface in the first model is reasoned to be due to the absence of a soil layer which is implemented in the next model (Chapter 3.3.2).

When the soil is increased to over 4 m in thickness, there is no additional improvement noticeable. The soil does not have any impact on the deeper isotherms. Only the 35 °C isotherm is affected, and it seems that when the soil gets to be over 4 m in thickness, it starts to act more like a heat sink than as an insulator. Lowering the conductivity of the soil will make it act as more of an insulator and improve the fit. None of the isotherms reach the same depth as the historical ones at the end of the simulation, and therefore the conductivity of granite is varied (Chapter 3.4.2).

The parameter sweep shows that with an increasing conductivity of granite, the final depth of the isotherms will approach the historical depth better, but near the surface, the 40 °C isotherm would show up. When looking at the 35 °C isotherm, the lower conductivities for both soil and granite produce better results. These contradicting results can be explained by the way it is modeled. The different layers present in the boreholes would have different thermal properties, and they all could be anisotropic with higher conductivities in a downward direction (Chapter 3.5.1).

The resurfaced technical drawings are used to create a 3D-model of the ground and water store. The main difference with the 2D-model is that this time, the higher soil conductivities produce higher R-square values for the 35 °C isotherm, with increasing conductivity of granite. However, with lower conductivities of granite, the lower conductivities of soil produce higher R-square values. It seems that with increasing conductivity of granite the heat is transported too fast, and so an increase in soil conductivity can make the soil act more like a heat sink in which some of the heat can escape, improving the R-square. With decreasing conductivity of granite the heat is not transported fast enough, and so a decrease in soil conductivity can serve as extra insulation. The maximum R-square values are also lower this time than for the 2D-model (Chapter 3.6.1). The water level is this time inside the soil layer as assumed from the technical drawings. To improve the overall fit, a lowering of the water level is investigated. With the water level lowered by 2 m, the results are very similar to the results of the 2D-model with even higher R-square values (Chapter 3.7.1).

5 Conclusion

The purpose of this thesis was to aid in the design of a thermal energy storage system for southern Finland that is economically feasible and has a high performance. To help achieve this goal a back-calculation of the underground thermal energy storage of the Kerava solar village has been performed to calibrate the models and increase the confidence level of the simulated results.

Most of the available historical data were in a graphical representation. There was data on the temperature changes inside the water store for each year, and on the change in depth of isotherms over time inside the surrounding rock mass. These graphs in combination with reported outside air temperatures formed the basis of the back-calculation (Figure 7, 8, and 9 in Chapter 3.1). Detailed technical drawings of the rock pit were not found. During the start of this research, there was no information on the geological setting of the site, but some were found later, describing the geological setting using drill data from 4 drill holes only (Figure 27, 28, and 29 in Chapter 3.5). This meant that the geometry of the rock pit and the geology was not fully defined.

The water store was modeled as a heat source, and the known temperature changes were used as input. The outside air temperature was modeled as a heat flux on the surface boundary, and the surrounding rock mass was given an initial temperature field according to the data. The simulated change in temperature of the surrounding rock mass was used as the output to which the historical data was compared.

The time period starting from the 1st of June until the 31st of August 1984 was chosen, in which the energy flows coming from the boreholes were small to non-existent, and their influence would be minimal (Table 2). Therefore, all the energy flows going in and out of the system were known.

A 2D-model was created that investigated the possible thickness of the soil (Chapter 3.4). Different soil thicknesses were simulated, and the results show that the replication of the historical data did not improve past a soil thickness of 4 m. Then the technical drawings surfaced that gave an idea on the geological surface, and it showed that at the location of interest the soil was 4 m thick which verified the modeled results.

When looking at the 35 °C isotherm only, an optimal fit was found with a conductivity of 2.8 and 1.0 W/(m·K) for granite and soil respectively. When looking at all isotherms, an optimum was reached with a conductivity of 6.5 and 1.0 W/(m·K) for granite and soil respectively. When looking at all isotherms except the 35 °C, an optimum was reached with a conductivity of 5.5 and 1.0 W/(m·K) for granite and soil respectively. However, the values for the conductivity of granite of over 4.0 W/(m·K) are unrealistic and produced the 40 °C isotherm near the surface which should not show up according to the data and thus the thermal parameters were unable to be quantified with confidence.

One of the main issues with the simulation was the scarcity of input data as discussed in the discussion chapter. There was not enough data to build a comprehensive model and

for that reason the results were unsatisfactory. When looking at different isotherms, the resulting best fitting thermal properties were conflicting and thus fail to achieve the objective, of quantifying the thermal properties, and the purpose of helping to calibrate the future models.

6 Recommendations

To validate future models to use in an optimization of the underground thermal energy storage in Finland the following should be attended to when choosing a project to use for the back-calculation including the boreholes:

- The project needs a well-documented history of all relevant temperatures, such as the temperatures inside the water store, the rock storage, and borehole fluids.
- The type of borehole heat exchanger should be known.
- The sensor placement should be precisely known.
- The hydrology of the site should be investigated.
- The geology should be known.
- The project should have detailed technical drawings of the underground constructions including materials used.

The project "Tackling the Challenges of a Solar-Community Concept in High Latitudes", of which this thesis is a part of, is focusing their research on combining a water pit storage with a borehole storage. To further this project, more research is needed, and some suggestions are given below:

- Perform a back-calculation of a project conforming specifications given before.
- Use calibrated model to perform numerical modeling and optimization of combined rock pit and borehole heat storage.

References

Chiasson, A. D., 2010. *Modeling Horizontal Ground Heat Exchangers in Geothermal Heat Pump Systems.* Boston, s.n.

Corradi, C., Schiavi, L., Rainieri, S. & Pagliarini, G., 2008. *Numerical Simulation of the Thermal Response Test Within Comsol Multiphysics® Environment.* Hannover, s.n.

Eppelbaum, L., Kutasov, I. & Pilchin, A., 2014. *Applied Geothermics.* s.l.:Springer Berlin Heidelberg.

Finnish Meteorological Institute, 2016. *Finnish Meteorological Institute.* [Online]
Available at: http:// http://en.ilmatieteenlaitos.fi/statistics-from-1961-onwards
[Accessed 13 May 2016].

Fryer, L. R., 1985. *Building Thermal Analysis for the Kerava Solar Village,* Helsinki: Helsinki University of Technology.

Google, 2016. *Google maps.* [Online]
Available at:
https://www.google.fi/maps/place/04200+Kerava/@62.2151928,23.5097716,7z/data=!4m5!3m4!1s0x46920062dd81505d:0x400b551554bb130!8m2!3d60.4009878!4d25.1020384
[Accessed 29 07 2016].

Honkonen, M., 2016. *Thermal energy storage concepts and their feasibility,* Helsinki: Aalto University School of Engineering.

Johansson, E., Acuña, J. & Palm, B., 2012. *Use of Comsol as a Tool in the Design of an Inclined Multiple Borehole Heat Exchanger.* Milan, s.n.

Kim, J. et al., 2010. Numerical modeling of aquifer thermal energy storage system. *Energy,* pp. 4955-4965.

Kukkonen, I., 2015. *Temperature Dependencies of Thermal Properties of Olkiluoto Rocks Measured with the Flash Method,* s.l.: University of Helsinki.

Kukkonen, I. T. & Peltoniemi, S., 1998. Relationships between Thermal and other Petrophysical. *Physics and Chemistry of the Earth,* pp. 341-349.

Lanini, S. et al., 2014. Improvement of borehole thermal energy storage design basedon experimental and modelling results. *Energy and Buildings,* pp. 393-400.

Lund, P., 1988. A hybrid thermal energy storage design. *Advances in solar energy technology,* Volume 1, pp. 1277-1281.

Lund, P. D., 1986. *Effect of Storage Thermal Behavior in Seasonal Storage Solar Heating Systems,* Helsinki: Helsinki University of Technology.

Lund, P. D., 1987. *Fundamentals of thermal Processes in a Hybrid Thermal Energy Storage,* Helsinki: Helsinki University of Technology.

Lund, P. D., Mäkinen, R. & Vuorelma, H., 1983. Simulation studies of the expected performance of Kerava Solar Village. *Energy Research,* pp. 347-357.

Lund, P. D., Peltola, S. S. & Routti, J. T., 1984. *Keravan aurinkokylän energiankäytön tutimus väliraportti lämpökeskuksen käyttöönottovaihe,* Helsinki: Helsinki University of Technology.

Mäkinen, R. & Lund, P. D., 1983. *Kerava Solar Village - A solar assisted heat pump system with long-term heat storage,* Helsinki: Helsinki University of Technology.

Nordell, B. & Hellström, G., 2000. High temperature solar heated seasonal storage system for low temperature heating of buildings. *Soal energy,* 69(6), pp. 511-523.

Novo, A. V., Bayon, J. R., Castro-Fresno, D. & Rodriquez-Hernandez, J., 2010. Review of seasonal heat storage in large basins: water tanks and gravel-water pits. *Applied Energy,* Volume 87, pp. 390-397.

Oberdorfer, P., Hu, R., Holzbecher, E. & Sauter, M., 2013. *A coupled FEM model for numerical simulation of rechargeable shallo geothermal BHE Systems.* Stanford, Stanford University.

Pavlov, G. K. & Olesen, B. W., 2011. *Seasonal ground solar thermal energy storage-review of systems and applications.* Dubrovnik, s.n.

Peippo, K. & Peltola, S., 1988. *Compiled data from Kerava Solar Village 1983 - 1986,* Helsinki: Helsinki University of Technology.

Peltola, S., 1986. *Keravan aurinkokylän lämmitysjärjestelmän mitattu ja simuloitu energiankäyttö,* Helsinki: Helsinki University of Technology.

Reuss, M., 2015. The use of borehole thermal energy storage (BTES) systems. *Advances in Thermal Energy Storage Systems: Methods and Applications,* pp. 117-147.

Reuss, M., Beuth, W., Schmidt, M. & Schoelkopf, W., 2006. *Solar district heating with seasonal storage in Attenkirchen,* s.l.: Bavarian Center of Applied Energy Research.

Robertson, E. C., 1988. *Thermal Properties of Rocks,* s.l.: United States Department of the Interior.

Schiavi, L., 2009. *3D Simulation of the Thermal Response Test in a U-tube Borehole Heat Exchanger.* Milan, s.n.

Sharma, S. D. & Sagara, K., 2005. Latent Heat Storage Materials and Systems: A. *International Journal of Green Energy,* pp. 1-56.

SITRA, 1980. *Lämpövaraston pohjavesiolosuhteet ja kallioperä,* Helsinki: OY VESI-HYDRO AB.

Suomen Rakennusinsinöörien Liitto RIL ry, 2013. *RIL 261-2013 Routasuojaus - rakennukset ja infrarakenteet,* Helsinki: RIL.

Appendices

Appendix 1   Rock temperatures surrounding the water store
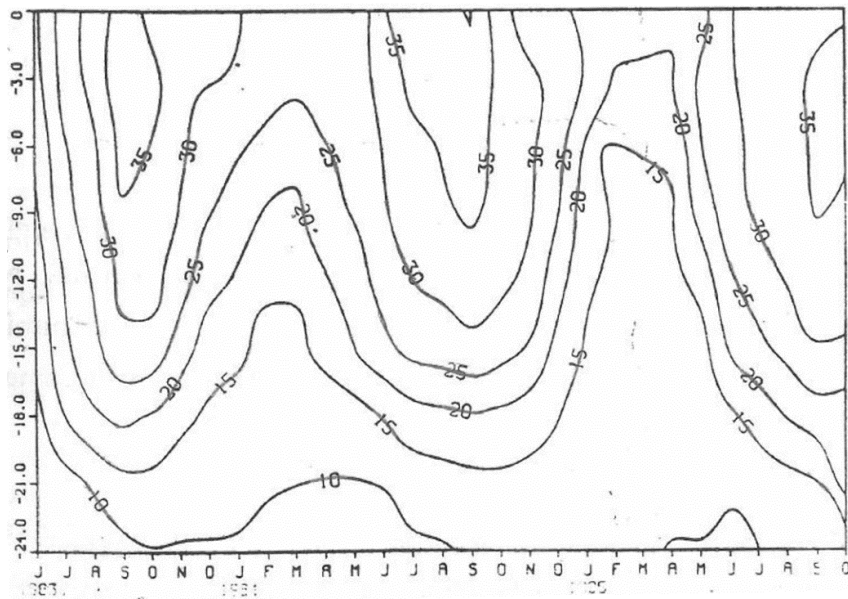
1 1. Isotherms of rock mass at 2m distance from water store in Northern direction from 1983-85 (Peltola, 1986)
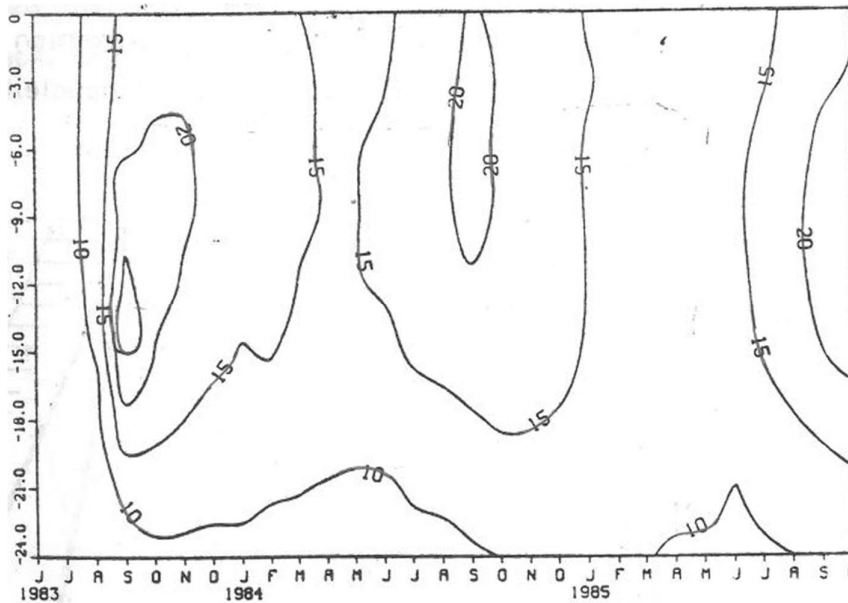
1 2. Isotherms of rock mass at 6m distance from water store in Northern direction from 1983-85 (Peltola, 1986)

1 3. Isotherms of rock mass at 10m distance from water store in Northern direction from 1983-85 (Peltola, 1986)

1 4. Isotherms of rock mass at 14m distance from water store in Northern direction from 1983-85 (Peltola, 1986)

Appendix 2   Temperatures of the water store

2 1. Temperatures of the water store changing with depth over time from the 1st of June until the 31st of August 1984. Temperatures given in °C

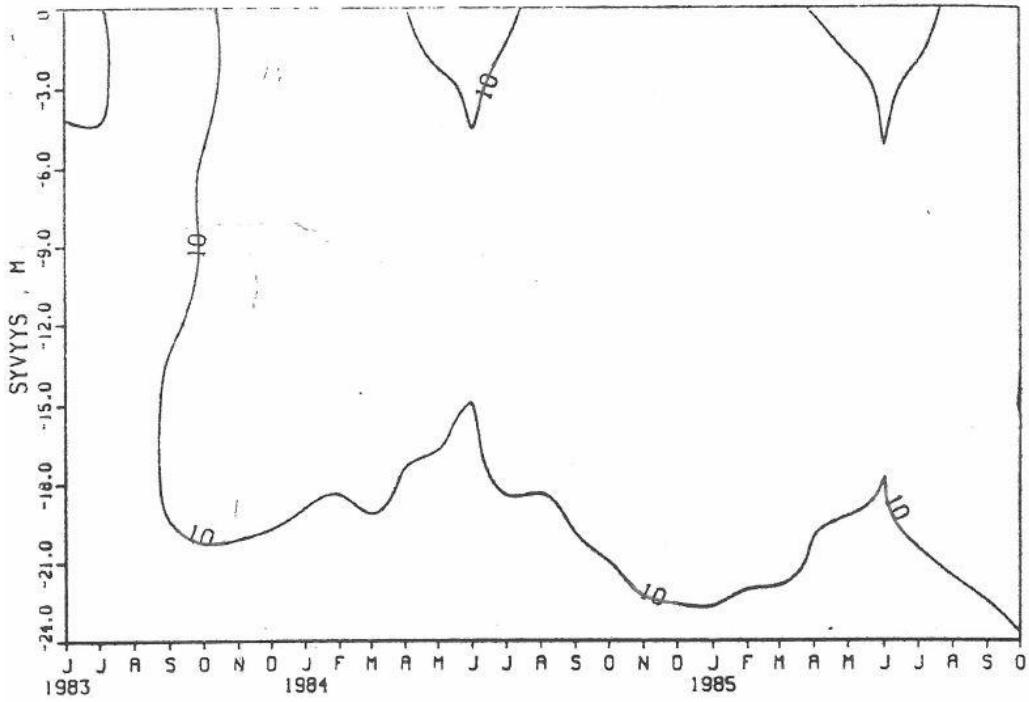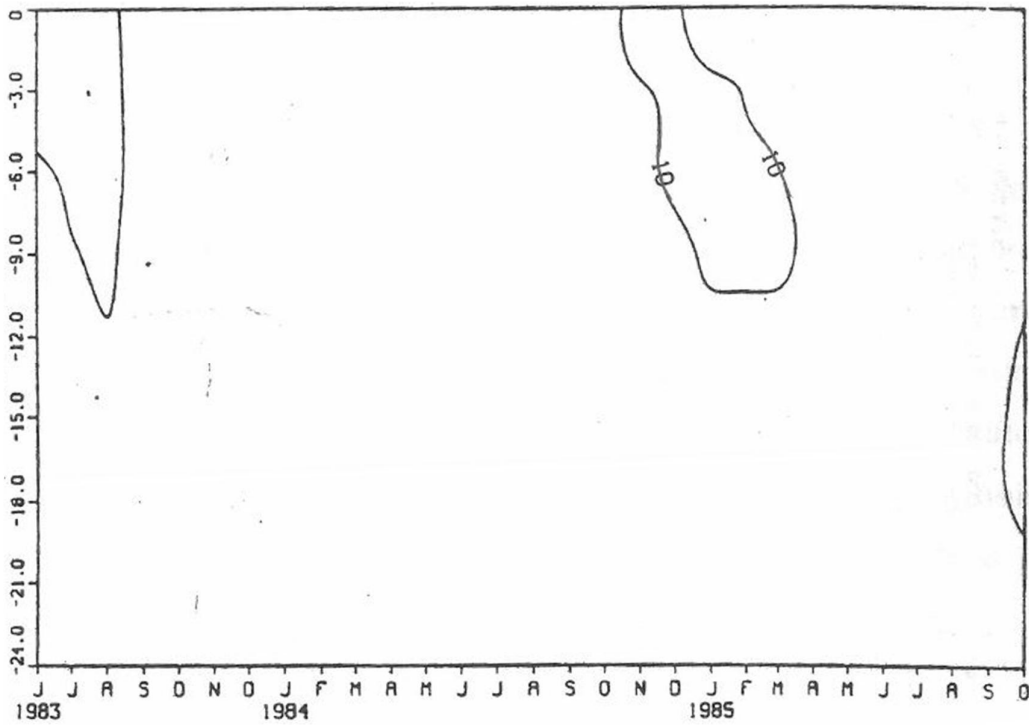| Day	0	-2	-4	-6	-8	-10	-12	-14	-16	-18	-20
						Depth (m)					
0	65	58.4	52.6	49.0	47.1	45.2	43.3	41.4	29.8	22.4	15
1	65	58.5	52.8	49.0	47.1	45.2	43.2	41.3	29.8	22.4	15
2	65	58.4	52.7	49.0	47.1	45.1	43.2	41.3	29.8	22.4	15
3	65	58.3	52.4	48.8	46.9	45.0	43.1	41.2	29.8	22.4	15
4	65	58.1	51.7	48.6	46.8	44.9	43.0	41.1	29.8	22.4	15
5	65	57.8	50.9	48.4	46.6	44.7	42.9	41.0	29.8	22.4	15
6	65	57.5	49.9	48.2	46.4	44.6	42.8	41.0	29.8	22.4	15
7	65	57.2	49.7	48.0	46.2	44.5	42.7	41.0	29.8	22.4	15
8	65	56.9	49.6	47.8	46.1	44.4	42.7	41.0	29.8	22.4	15
9	65	56.8	49.5	47.8	46.1	44.4	42.7	41.0	29.8	22.4	15
10	65	56.9	49.6	47.9	46.1	44.4	42.7	41.0	29.8	22.4	15
11	65	57.2	49.7	48.0	46.3	44.5	42.8	41.1	29.8	22.4	15
12	65	57.6	50.0	48.2	46.4	44.7	42.9	41.2	29.8	22.4	15
13	65	57.9	51.1	48.5	46.7	44.9	43.1	41.3	29.8	22.4	15
14	65	58.2	52.2	48.8	46.9	45.1	43.2	41.4	29.8	22.4	15
15	65	58.5	53.0	49.1	47.2	45.3	43.4	41.4	29.8	22.4	15
16	65	58.6	53.6	49.4	47.4	45.5	43.5	41.5	29.8	22.4	15
17	65	58.7	54.0	49.7	47.6	45.6	43.5	41.5	29.8	22.4	15
18	65	58.8	54.2	49.8	47.7	45.6	43.6	41.5	29.8	22.4	15
19	65	58.8	54.2	49.8	47.7	45.6	43.5	41.4	29.8	22.4	15
20	65	58.8	54.1	49.7	47.6	45.5	43.4	41.3	29.8	22.4	15
21	65	58.7	53.9	49.6	47.5	45.4	43.3	41.2	29.8	22.4	15
22	65	58.6	53.6	49.4	47.3	45.3	43.2	41.1	29.8	22.4	15
23	65	58.5	53.2	49.2	47.2	45.1	43.1	41.1	29.8	22.4	15
24	65	58.4	52.8	49.0	47.0	45.0	43.0	41.0	29.8	22.4	15
25	65	58.2	52.4	48.8	46.9	44.9	43.0	41.0	29.8	22.4	15
26	65	58.1	52.1	48.7	46.8	44.9	42.9	41.0	29.8	22.4	15
27	65	58.1	51.9	48.7	46.8	44.9	43.0	41.1	29.8	22.4	15
28	65	58.1	52.0	48.7	46.8	44.9	43.0	41.1	29.8	22.4	15
29	65	58.2	52.2	48.8	46.9	45.0	43.1	41.2	29.8	22.4	15
30	65	58.4	52.7	49.0	47.1	45.2	43.3	41.3	29.8	22.4	15
31	65	58.6	53.4	49.3	47.4	45.4	43.4	41.5	29.8	22.4	15
32	65	58.9	54.3	49.8	47.8	45.8	43.7	41.7	29.8	22.4	15
33	65	59.2	55.2	51.1	48.4	46.2	44.1	41.9	29.8	22.4	15
34	65	59.4	55.8	52.2	49.1	46.8	44.4	42.1	29.8	22.4	15
35	65	59.5	56.1	52.8	49.6	47.2	44.7	42.2	29.8	22.4	15
36	65	59.5	56.2	52.9	49.7	47.2	44.7	42.2	29.8	22.4	15
37	65	59.4	56.0	52.6	49.5	47.0	44.6	42.2	29.8	22.4	15
38	65	59.3	55.8	52.3	49.2	46.8	44.4	42.0	29.9	22.4	15

Day	Depth (m)										
	0	-2	-4	-6	-8	-10	-12	-14	-16	-18	-20
39	65	59.2	55.6	52.0	49.0	46.6	44.3	41.9	29.9	22.4	15
40	65	59.1	55.5	51.9	48.9	46.5	44.2	41.8	29.9	22.4	15
41	65	59.0	55.5	51.9	48.9	46.5	44.1	41.7	29.9	22.4	15
42	65	59.0	55.4	51.9	48.9	46.4	44.0	41.6	29.9	22.4	15
43	65	59.0	55.4	51.8	48.8	46.4	43.9	41.5	29.9	22.4	15
44	65	59.0	55.4	51.7	48.7	46.3	43.8	41.4	29.9	22.5	15
45	65	59.0	55.3	51.5	48.6	46.2	43.7	41.3	29.9	22.5	15
46	65	59.0	55.1	51.3	48.4	46.0	43.6	41.3	29.9	22.5	15
47	65	58.9	55.0	51.0	48.2	45.9	43.6	41.2	29.9	22.5	15
48	65	58.9	54.8	50.7	48.1	45.8	43.5	41.2	29.9	22.5	15
49	65	58.8	54.6	50.4	47.9	45.7	43.5	41.2	30.0	22.5	15
50	65	58.7	54.4	50.1	47.9	45.7	43.5	41.2	30.0	22.5	15
51	65	58.7	54.3	50.0	47.8	45.7	43.5	41.3	30.0	22.5	15
52	65	58.7	54.4	50.0	47.9	45.7	43.6	41.4	30.0	22.5	15
53	65	58.8	54.5	50.2	48.0	45.8	43.7	41.5	30.0	22.5	15
54	65	58.9	54.8	50.6	48.2	46.0	43.8	41.6	30.1	22.5	15
55	65	59.0	55.1	51.1	48.4	46.2	44.0	41.8	30.2	22.5	15
56	65	59.2	55.4	51.7	48.8	46.5	44.2	41.9	30.4	22.5	15
57	65	59.3	55.8	52.3	49.2	46.8	44.4	42.1	30.6	22.5	15
58	65	59.4	56.1	52.7	49.6	47.1	44.7	42.2	31.0	22.5	15
59	65	59.4	56.3	53.1	50.0	47.4	44.9	42.3	31.3	22.5	15
60	65	59.4	56.4	53.4	50.3	47.7	45.0	42.4	31.4	22.6	15
61	65	59.4	56.4	53.5	50.5	47.8	45.1	42.4	31.4	22.6	15
62	65	59.3	56.4	53.5	50.5	47.8	45.1	42.4	31.3	22.6	15
63	65	59.2	56.3	53.4	50.4	47.7	45.0	42.3	31.1	22.6	15
64	65	59.1	56.1	53.2	50.2	47.5	44.8	42.2	31.0	22.6	15
65	65	59.0	56.0	52.9	49.8	47.2	44.6	42.0	30.9	22.6	15
66	65	58.9	55.8	52.6	49.6	47.0	44.4	41.9	30.8	22.6	15
67	65	58.8	55.6	52.4	49.3	46.8	44.3	41.7	30.7	22.6	15
68	65	58.7	55.4	52.2	49.1	46.6	44.1	41.6	30.7	22.6	15
69	65	58.7	55.4	52.1	49.1	46.6	44.0	41.5	30.6	22.6	15
70	65	58.6	55.3	52.0	49.0	46.5	44.0	41.5	30.6	22.6	15
71	65	58.6	55.3	52.0	49.0	46.5	44.0	41.4	30.6	22.6	15
72	65	58.6	55.3	52.1	49.0	46.5	44.0	41.4	30.6	22.6	15
73	65	58.6	55.3	52.1	49.1	46.5	44.0	41.4	30.6	22.6	15
74	65	58.6	55.3	52.1	49.1	46.5	44.0	41.4	30.6	22.6	15
75	65	58.6	55.4	52.1	49.1	46.5	44.0	41.4	30.6	22.6	15
76	65	58.6	55.4	52.1	49.1	46.6	44.0	41.5	30.6	22.6	15
77	65	58.7	55.5	52.3	49.2	46.7	44.1	41.5	30.6	22.6	15
78	65	58.7	55.6	52.4	49.4	46.8	44.2	41.6	30.6	22.6	15
79	65	58.7	55.7	52.7	49.7	47.0	44.4	41.7	30.6	22.6	15
80	65	58.8	55.9	53.0	50.1	47.3	44.6	41.9	30.7	22.6	15

Day	Depth (m)										
	0	-2	-4	-6	-8	-10	-12	-14	-16	-18	-20
81	65	58.8	56.0	53.2	50.5	47.6	44.8	42.0	30.7	22.6	15
82	65	58.9	56.2	53.5	50.8	48.0	45.1	42.2	30.7	22.6	15
83	65	58.9	56.3	53.7	51.1	48.3	45.3	42.4	30.7	22.6	15
84	65	58.9	56.4	53.8	51.3	48.5	45.5	42.5	30.6	22.5	15
85	65	58.9	56.4	53.9	51.3	48.6	45.6	42.6	30.5	22.5	15
86	65	58.9	56.3	53.8	51.3	48.5	45.5	42.6	30.3	22.5	15
87	65	58.9	56.3	53.7	51.1	48.3	45.4	42.5	30.0	22.5	15
88	65	58.8	56.1	53.4	50.7	48.0	45.2	42.4	30.0	22.5	15
89	65	58.7	55.9	53.0	50.2	47.5	44.9	42.3	29.9	22.5	15
90	65	58.6	55.6	52.5	49.5	47.0	44.6	42.1	29.9	22.4	15
91	65	58.5	55.2	51.9	48.9	46.6	44.2	41.9	29.8	22.4	15